J. Fluid Mech. (2003), *vol.* 480, *pp.* 233–265. © 2003 Cambridge University Press
DOI: 10.1017/S0022112003003744 Printed in the United Kingdom

Integral methods for shallow free-surface flows with separation

By SHINYA WATANABE[1], VACHTANG PUTKARADZE[2] AND TOMAS BOHR[3]

[1]Department of Mathematical Sciences, Ibaraki University, 310-8512 Mito, Japan

[2]Department of Mathematics and Statistics, University of New Mexico, Albuquerque, NM 87131-1141, USA

[3]Department of Physics, The Technical University of Denmark, Kgs. Lyngby, DK-2800, Denmark

(Received 21 August 2000 and in revised form 30 September 2002)

We study laminar thin film flows with large distortions of the free surface, using the method of averaging across the flow. Two specific problems are studied: the circular hydraulic jump and the flow down an inclined plane. For the circular hydraulic jump our method is able to handle an internal eddy and separated flow. Assuming a variable radial velocity profile as in Kármán–Pohlhausen's method, we obtain a system of two ordinary differential equations for stationary states that can smoothly go through the jump. Solutions of the system are in good agreement with experiments. For the flow down an inclined plane we take a similar approach and derive a simple model in which the velocity profile is not restricted to a parabolic or self-similar form. Two types of solutions with large surface distortions are found: solitary, kink-like propagating fronts, obtained when the flow rate is suddenly changed, and stationary jumps, obtained, for instance, behind a sluice gate. We then include time dependence in the model to study the stability of these waves. This allows us to distinguish between sub- and supercritical flows by calculating dispersion relations for wavelengths of the order of the width of the layer.

1. Introduction

In this paper we develop a simple quantitative method to describe flows with a free surface which can undergo large distortions. Our method is capable of handling flows whose velocity profile may become far from parabolic — even including separation and regions of reverse flow. We are concerned with the case when the fluid layer is thin. For low Reynolds number flows the lubrication approximation and asymptotic long-wave theory can be used with great success (see Oron, Davis & Bankoff 1997 for a review). For high Reynolds number flows without separation an inviscid approximation and the shallow water equations (Whitham 1974) are widely used. For moderate Reynolds numbers where these limiting approximations are invalid it is important to take both inertial and viscous effects into account in a consistent way, and yet one would like to keep the model simple enough to be tractable. Integral methods, like the ones developed by von Kármán, have been the practical choice in this regime (Prokopiou, Cheng & Chang 1991). Despite the *ad hoc* nature of the methods which requires an assumption of a velocity profile, they have led to useful quantitative predictions of thin flows. The assumed velocity profiles have traditionally been such simple ones as a flat velocity profile or a parabolic one

https://doi.org/10.1017/S0022112003003744 Published online by Cambridge University Press

(Prokopiou *et al.* 1991) which remain self-similar in the flow direction. However, the velocity profile may change when there is a free surface with large distortions. In this paper we show that an integral method with a more flexible velocity profile can handle a class of such problems successfully.

To be specific we develop the method in the context of two physical examples: the *circular hydraulic jump* and the *flow down an inclined plane*. Both geometries support jump- or kink-like solutions with abrupt changes in the surface shape and internal velocity profiles. Analytical solutions for such flows are extremely difficult to obtain, and simple approximate theories that capture the phenomena are invaluable.

The two flows are studied in § 2 and § 3, respectively. In § 2 we develop the theory for the circular hydraulic jump. We first study the boundary layer approximation to the full Navier–Stokes equations, and reduce it to a simple set of equations by averaging over the thickness. Stationary solutions are obtained by solving a two-point boundary value problem for a system of only two ordinary differential equations. The solution is compared to previous experiments, showing good agreement. Taking advantage of the simplicity of the reduced equations, it is possible to obtain analytic approximations for the stationary solution. Two 'outer' solutions connected by an 'inner' transition region are studied separately and we obtain a relationship analogous to the shock condition in the classical shock theory, but within our viscous model.

The flow down an inclined plane is then studied in § 3. We use the same strategy as in § 2 to derive a simple model for the two-dimensional flow, then seek stationary solutions approaching the equilibrium Nusselt flow far downstream. We demonstrate that a family of solutions with a sudden change in the surface can be found only when flexibility is introduced in the assumptions for the velocity profile. In contrast no such solution can be found with a self-similar velocity profile. These solutions correspond to the circular hydraulic jump in the case of the radial geometry, and can be interpreted as the stationary hydraulic jump created behind a sluice gate in a river although turbulence is not included in the model. Unlike the equilibrium flow downstream, the upstream part of the flow is a transient expanding flow with a linear growth in thickness. The velocity profile departs considerably from parabolic near the jump.

It is not easy to analyse the stability of the solutions with jumps. In § 3.4 we take the equilibrium flow down the inclined plane, and study its linear stability. A well-established concept in the inviscid theory is to classify flows as super- and subcritical when the thickness is small and large, respectively. They do not have obvious counterparts, however, when viscosity is included. By looking carefully at the dispersion relation in the long and medium wave regime, we can classify a stationary flow into these two categories in our viscous model. Unfortunately, the model shows spurious divergences in the short-wavelength region which we do not know how to overcome at present. This makes the model suited only for stationary situations.

The Appendix describes details of the calculations in § 3. In addition, we show that our simple model is capable of handling the kink-like travelling wave solutions studied in the previous literature that occur, for instance, when the flow rate is suddenly changed. Their velocity profiles are found to stay close to parabolic even when they are allowed to vary. Therefore, they are qualitatively simpler to describe than the hydraulic jumps.

A letter describing the assumptions of our method and some of the main results appeared elsewhere (Bohr, Putkaradze & Watanabe 1997). During the referee process of the present manuscript, an article by Ruschak & Weinstein (2001) appeared which used the same assumptions as ours, apparently without noticing our earlier work,

https://doi.org/10.1017/S0022112003003744 Published online by Cambridge University Press

and analysed the flow down an inclined plane, corresponding to a part of § 3 of this article. Although the derived model is identical, we study the linear stability of the equilibrium flow while they compare predictions from the model with experiments and full numerics of the Navier–Stokes and the boundary layer equations. We have added a few notes regarding their work in § 3.

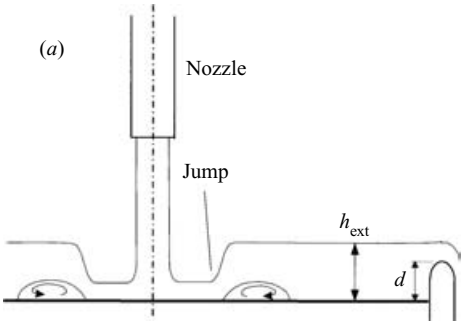
2. The circular hydraulic jump

2.1. *Introduction to the problem*

When a jet of fluid hits a flat horizontal surface, the fluid spreads out radially in a thin, rapidly flowing layer. At a certain distance from the jet a sudden thickening of the flow takes place, which is called the circular hydraulic jump. This is commonly seen in the kitchen sink, but it is also important as a coating flow and in jet cooling of a heated surface (Liu & Lienhard 1993). In these practical flows with typically high Reynolds numbers, disturbances often make the jump non-stationary and distorted. In controlled laboratory experiments corresponding to a more moderate Reynolds number, an apparently stationary, radially symmetric flow can be achieved. Experiments on the circular hydraulic jumps have been carried out by many researchers (for instance, Tani 1949; Olsson & Turkdogan 1966; Ishigai *et al.* 1977; Nakoryakov, Pokusaev & Troyan 1978; Craik *et al.* 1981), but we mostly refer to measurements of C. Ellegaard and coworkers (Bohr *et al.* 1996, 1998; Ellegaard *et al.* 1998, 1999; Marcussen 1999) since their Reynolds numbers were moderate and the flows were laminar as we assume here. In addition, they measured both velocity and height dependence as a function of radius. We thank them for providing us with data and pictures. A schematic view and a video image of the circular jump are shown in figure 1.

In these experiments the hydraulic jump is formed on a flat disc with a circular rim. The rim height d can be varied, and is an important control parameter. Since the rim is located far from the impinging jet as the diameter of the disc is around 36 cm, it does not affect the jump except that it changes the height of the fluid layer h_{ext} exterior to the jump. The jump still forms even when $d = 0$, but a larger d makes h_{ext} larger and, therefore, the jump stronger. Typically, h_{ext} exceeds d by 1–2 mm. The surface profiles for varying d are shown in figure 2. An interesting transition in the flow structure has been observed (Bohr *et al.* 1996, 1998) as d is varied. For $d = 0$, it was noticed (Tani 1949; Olsson & Turkdogan 1966; Ishigai *et al.* 1977; Nakoryakov *et al.* 1978; Craik *et al.* 1981) that the jump contains an eddy on the bottom, called a *separation bubble*, whose inner edge is located very close to the position of the abrupt change on the surface, as illustrated in figure 3(*a*). Such a hydraulic jump is referred to as a *type I* jump. While d remains small, this jump is stable, but as d is increased, a *wave-breaking* transition occurs (Bohr *et al.* 1996, 1998) which results in another state of the flow. In this *type II* state, the flow has an additional eddy, called a *roller* or a *surfing wave*, just under the surface as shown in figure 3(*b*). (If d is increased even further, the jump 'closes' as seen in figure 2.) This type II state was observed before (e.g. in Liu & Lienhard 1993), but the Reynolds number was too large to show the transition. The state resembles a broken wave in the ocean, but is still apparently laminar. On reducing d, the type I pattern reappears, and there is almost no hysteresis associated with this transition. The transition from type I to II often leads also to breaking of the radial symmetry. An intriguing set of polygonal jumps (Ellegaard *et al.* 1998, 1999) are created rather than the circular one. In this paper we shall concentrate on the type I flow which already poses considerable difficulties.

https://doi.org/10.1017/S0022112003003744 Published online by Cambridge University Press



(b)

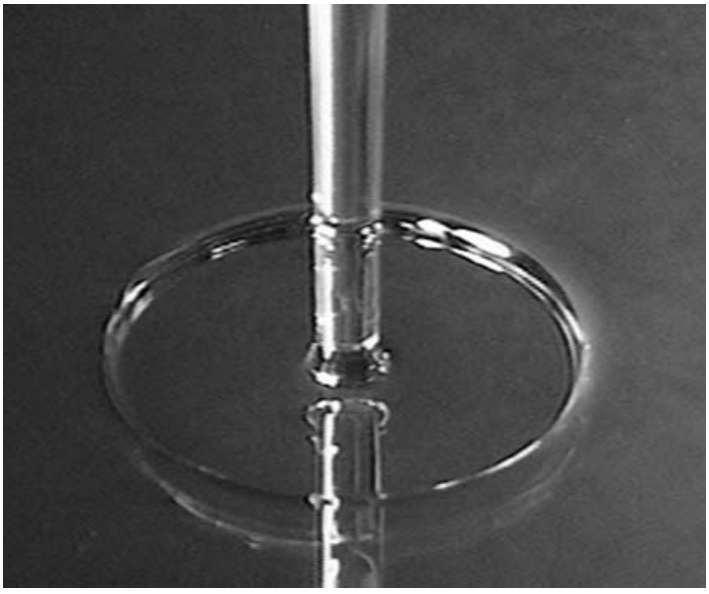


FIGURE 1. (*a*) Schematic view of the circular hydraulic jump. (*b*) Snapshot of a nearly perfect stationary and circular hydraulic jump. Ethylene-glycol is the liquid.

We hope to be able to generalize our approach in the future to be able to handle the transition to the type II flow.

Considering how simple and common the circular hydraulic jump appears to be, it is surprising that a satisfactory systematic theory does not exist. The approach considered as the standard for the study of hydraulic jumps is to combine the inviscid shallow water equation with Rayleigh's shocks (Chow 1959). In the beginning of the century Lord Rayleigh treated (Rayleigh 1914) a discontinuity in a one-dimensional linear flow geometry. Such a structure is usually called a *river bore* if it is moving and a *hydraulic jump* if it is stationary and is created due to, for example, variations in the river bed. His approach was based upon the analogy between shallow water theory and gas theory (Whitham 1974). He assumed that, across such a shock, the mass and momentum flux are conserved but not the energy flux.

In a coordinate system moving with the shock, the flow velocity v_1 and height h_1 upstream of the jump as well as v_2 and h_2 downstream of the jump are taken to be positive constant values. Then, conservation of mass flux Q across the jump is given by

https://doi.org/10.1017/S0022112003003744 Published online by Cambridge University Press

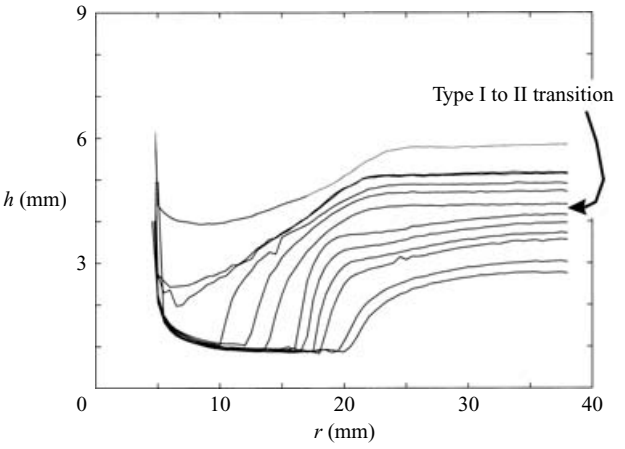


FIGURE 2. Height profiles $h(r)$ for different values of the external height h_{ext}. (The rim height d is controlled but not shown.) The height $h(r)$ approaches h_{ext} for large values of r. Parameters are: the flow rate $Q = 27\,\text{ml}\,\text{s}^{-1}$ and viscosity $\nu = 7.6 \times 10^{-6}\,\text{m}^2\,\text{s}^{-1}$, corresponding to the characteristic scales: radius $r_* = 2.8\,\text{cm}$, height $h_* = 1.4\,\text{mm}$, and radial velocity $u_* = 12\,\text{cm}\,\text{s}^{-1}$. Figure taken from Bohr *et al.* (1996).

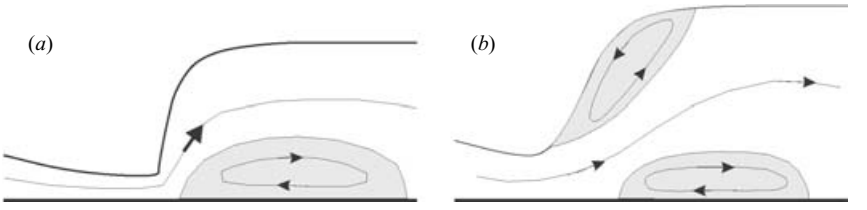


FIGURE 3. A schematic picture showing two observed flow patterns: (*a*) type I flow, with a separation bubble, which occurs for small d, and (*b*) type II flow, with an additional roller eddy, for large d. Transitions between these states occur at a certain d, with surprisingly small hysteresis.

$v_1 h_1 = v_2 h_2 = Q$. Conservation of momentum flux is $h_1(v_1^2 + gh_1/2) = h_2(v_2^2 + gh_2/2)$. These shock conditions lead to the relation

$$h_2/h_1 = \left(-1 + \sqrt{1 + 8F_1^2}\right)/2 = 2/\left(-1 + \sqrt{1 + 8F_2^2}\right), \tag{2.1}$$

where $F_1 = \sqrt{v_1^2/gh_1} = (h_c/h_1)^{3/2}$ and $F_2 = \sqrt{v_2^2/gh_2} = (h_c/h_2)^{3/2}$ are the upstream and downstream Froude numbers, respectively, and $h_c = (Q^2/g)^{1/3}$ is called the critical height. It is easy to see that h_c is always between h_1 and h_2, and that $F_1 > 1 > F_2$ if $h_1 < h_c < h_2$, and $F_1 < 1 < F_2$ if $h_1 > h_c > h_2$. In other words the jump connects a *supercritical flow* with $F > 1$ on the shallower side ($h < h_c$) to a *subcritical flow* with $F < 1$ on the deeper side ($h > h_c$). Since the Froude number measures the ratio of the fluid velocity v and the velocity of linear surface waves $\sqrt{gh}$, it means that, in the moving frame, the flow moves more rapidly than the surface waves on the shallower side, but moves slower on the deeper side — in a precise analogy with the gas theory (Stoker 1957; Whitham 1974). Further, it is found that the upstream h_1 must be supercritical by considering the change in the energy flux across the jump (Whitham 1974):

$$Q_{e2} - Q_{e1} = -g\,Q(h_2 - h_1)^3/(8\pi h_1 h_2), \tag{2.2}$$

https://doi.org/10.1017/S0022112003003744 Published online by Cambridge University Press

where Q_e denotes the energy flux. Since the energy must be dissipated through the jump, i.e. $Q_{e2} - Q_{e1} < 0$, rather than generated, it is required that $h_1 < h_2$. The origin of the dissipation is usually attributed to the turbulent motions at the discontinuity and surface waves carrying energy away from it.

It is possible to apply this theory, combined with an assumption of the potential flow, to describe the circular hydraulic jump. However, it leads to incorrect estimates (Watson 1964; Bohr, Dimon & Putkaradze 1993) of the radius of the jump r_{jump}. Most notably, r_{jump} is predicted to be sensitive to the radius of the impinging jet, which should be greatly influenced by the radius and height of the inlet nozzle where liquid comes out. In experiments (Watson 1964; Bohr *et al.* 1993) such a strong tendency was not observed. Instead, it has been found that r_{jump} scales with the flow rate Q with a certain power, and this supports a model in which viscosity plays an important role. Watson (1964) constructed a model of the flow consisting of the inviscid and viscous regimes, and solved the viscous part assuming a similarity profile. By connecting to the specified external height h_{ext} via a Rayleigh shock, he obtained a prediction for the radius of the jump which compares favourably with the measurements (Watson 1964; Bohr *et al.* 1993), as we explain in § 2.5. In his model the viscous layer starts from the stagnation point at $r = 0$ on the plate and quickly reaches the surface at a small r. There is a fairly long region from this r to r_{jump} in which the flow is fully viscous.† Thus, one could neglect the inviscid region and assume a fully viscous flow everywhere in order to derive a simpler model. This assumption was made by Kurihara (1946) and Tani (1949) who started from the boundary layer equations developed by Prandtl (Prandtl 1904; Schlichting 1979). They took an average of the equations over the thickness, also assuming a similarity velocity profile. This resulted in a single ordinary differential equation for the stationary jump. This theory was elaborated in Bohr *et al.* (1993) who realized that the flow outside the jump would naturally lead to a singularity at a large r. By identifying this singularity with the outflow over the rim of the plate, the flow outside the jump could be uniquely specified. By introducing a Rayleigh shock, the jump radius and its parameter dependence was calculated and compared to measurements. The model predicted the observed r_{jump} reasonably well, as we review in §§ 2.2–2.5.

Obviously, treating the jump as a discontinuity provides us with no information on the internal structure of the jump region, such as the type I to II transition of the flow patterns. It also seems inconsistent to assume a Rayleigh shock when viscous loss occurs in the whole domain. Why do we assume an extra energy loss at the 'jump' where the flow is stationary and apparently laminar? It seems possible to attribute the energy dissipation entirely to laminar viscous forces, and to construct a viscous theory which produces a smooth but kink-like surface shape without the need for a discontinuity. Nevertheless, such a description must overcome a difficulty arising from the Goldstein-type singularity (Goldstein 1948; Landau & Lifshitz 1987) of the boundary layer equations in the vicinity of separation points. This singularity is thought to be an artificial one created by truncation of higher derivatives from the Navier–Stokes equations. It also arises in the 'usual' boundary layer situation where a high Reynolds number flow passes over a body such as a wing. Here substantial progress has been achieved by studying the modification of the free-stream flow

† This assumption is confirmed by recent laser-Doppler measurements of the velocity profile before the jump (Marcussen 1999). Thus, the assumption, made by Godwin (1993), Blackford (1996), and Brechet & Néda (1999), that the jump occurs at the point where the growing viscous layer touches the surface and the flow becomes fully developed, is incorrect.

https://doi.org/10.1017/S0022112003003744 Published online by Cambridge University Press

caused by the growing boundary layer, which has led to the discovery of the triple-deck structure at high Reynolds numbers and the inverse method, where the boundary layer thickness is found iteratively (Carter & Wornom 1975; Sobey 2000).

A similar approach for free surface flows has been used by Smith and coworkers (Gajjar & Smith 1983; Bowles & Smith 1992) and Higuera (1994, 1997). They found that, without the free-stream flow above the free surface, it is still possible to modify the boundary layer iteratively by taking the pressure gradient across the layer into account. The height of the free surface enters the equations through the hydrostatic pressure. Higuera (1994, 1997) numerically solved such a system of the boundary layer equations with a free surface, and showed that it is possible to avoid a singularity.

In the present work we propose a way to resolve the problem in order to obtain a simpler system that describes this coupling mechanism. We first include an additional degree of freedom in the velocity profile to make it non-self-similar, as in the Kármán–Pohlhausen method (Grimson 1976) for the usual boundary layer theory. To describe the evolution, in r, of this free parameter, we couple the layer thickness to the pressure by assuming hydrostatic pressure, as in the previous work mentioned (Gajjar & Smith 1983; Bowles & Smith 1992; Higuera 1994, 1997). The resulting model for a stationary solution is two coupled ordinary differential equations, and reproduces the type I flow with a separation bubble — the one shown in figure 3(a). Comparison with the experiment is made in § 2.7. It is possible to approximate analytically the stationary solution found in the model. In § 2.8 the analysis is presented separately for the regions before and after the jump (i.e. two 'outer' solutions) and the 'inner' solution inside the jump region. An interesting observation on the inner solution is that a formal parameter β can be introduced, where $\beta = 1$ corresponds to our model, whereas Rayleigh's shock condition is recovered in the limit $\beta \to 0$.

2.2. *The full model*

We write down the complete model to describe the circular hydraulic jump under the assumption that the flow is laminar and radially symmetric without any angular velocity component. We take the radial and vertical coordinates $\tilde{r}$ and $\tilde{z}$, and denote the velocity components by $\tilde{u}$ and $\tilde{w}$, respectively. We use tildes for the dimensional variables, dependent or independent. Dimensionless variables will be expressed by the same symbols but without tildes. In figures, however, we do not use tildes for simplicity. The governing equations are the continuity equation

$$\tilde{u}_{\tilde{r}} + \tilde{u}/\tilde{r} + \tilde{w}_{\tilde{z}} = 0 \tag{2.3}$$

and the Navier–Stokes equations

$$\tilde{u}_{\tilde{t}} + \tilde{u}\tilde{u}_{\tilde{r}} + \tilde{w}\tilde{u}_{\tilde{z}} = -\tilde{p}_{\tilde{r}}/\rho + \nu(\tilde{u}_{\tilde{r}\tilde{r}} + \tilde{u}_{\tilde{r}}/\tilde{r} - \tilde{u}/\tilde{r}^2 + \tilde{u}_{\tilde{z}\tilde{z}}), \tag{2.4a}$$

$$\tilde{w}_{\tilde{t}} + \tilde{u}\tilde{w}_{\tilde{r}} + \tilde{w}\tilde{w}_{\tilde{z}} = -\tilde{p}_{\tilde{z}}/\rho - g + \nu(\tilde{w}_{\tilde{r}\tilde{r}} + \tilde{w}_{\tilde{r}}/\tilde{r} + \tilde{w}_{\tilde{z}\tilde{z}}), \tag{2.4b}$$

where subscripts denote partial differentiation such as $\tilde{u}_{\tilde{t}} = \partial\tilde{u}/\partial\tilde{t}$. For the boundary conditions we impose no slip on the bottom: $\tilde{u}(\tilde{z} = 0) = \tilde{w}(\tilde{z} = 0) = 0$ and the dynamic boundary conditions on the free surface $\tilde{z} = \tilde{h}(\tilde{t}, \tilde{r})$:

$$\tilde{p} - \frac{2\rho\nu}{1 + \tilde{h}_{\tilde{r}}^2}\left\{\tilde{h}_{\tilde{r}}^2\tilde{u}_{\tilde{r}} + \tilde{w}_{\tilde{z}} - 2\tilde{h}_{\tilde{r}}(\tilde{w}_{\tilde{r}} + \tilde{u}_{\tilde{z}})\right\}\Big|_{\tilde{z}=\tilde{h}} = \sigma\tilde{k}, \tag{2.5a}$$

$$\nu\left\{\left(\tilde{h}_{\tilde{r}}^2 - 1\right)(\tilde{w}_{\tilde{r}} + \tilde{u}_{\tilde{z}}) - 2\tilde{h}_{\tilde{r}}(\tilde{u}_{\tilde{r}} - \tilde{w}_{\tilde{z}})\right\}\Big|_{\tilde{z}=\tilde{h}} = 0, \tag{2.5b}$$

where σ is the coefficient of surface tension and $\tilde{k}$ is the mean local curvature of the free surface. We also need to satisfy the kinematic boundary condition on the free

https://doi.org/10.1017/S0022112003003744 Published online by Cambridge University Press

surface: $\tilde{h}_{\tilde{t}} + \tilde{u}\tilde{h}_{\tilde{r}} = \tilde{w}$ on $\tilde{z} = \tilde{h}(\tilde{t}, \tilde{r})$. We are mostly interested in stationary solutions in this section. When the flow is stationary, we may integrate (2.3) over $\tilde{z}$ from 0 to $\tilde{h}$, and use the kinematic condition to obtain

$$\tilde{r} \int_0^{\tilde{h}(\tilde{r})} \tilde{u}(\tilde{r}, \tilde{z})\, \mathrm{d}\tilde{z} = q = Q/(2\pi). \tag{2.6}$$

This quantity, the total mass flux Q or the mass flux per angle q, is a constant, given as a parameter in the experiment.

2.3. *Boundary layer approximation*

Since it is a formidable task to treat the full model as it stands, some simplifications need to be made. As explained in § 1, the Reynolds number for the flow of the circular hydraulic jump is too large to justify the lubrication approximation, but is not large enough to use the inviscid approximation. Fortunately, the flow is 'thin', i.e. runs predominantly horizontally along the plate. Truncation of the full model by the boundary layer approximation is quite natural in such a situation, and has indeed been done in previous work (Kurihara 1946; Tani 1949; Bohr *et al.* 1993). In the boundary layer approximation pressure, viscous and inertial terms in (2.4) are all assumed to be of the same order, but there are only a few dominant terms in each group. For instance, a viscous term $\nu\tilde{u}_{\tilde{r}\tilde{r}}$ is assumed to be negligible compared to $\nu\tilde{u}_{\tilde{z}\tilde{z}}$. The dominant terms in (2.4*a*) are determined in the usual manner: $\tilde{u}_{\tilde{t}}$ (if time dependent), inertia terms $\tilde{u}\tilde{u}_{\tilde{r}}$ and $\tilde{w}\tilde{u}_{\tilde{z}}$, the pressure term $\tilde{p}_{\tilde{r}}/\rho$, and the dominant viscous term $\nu\tilde{u}_{\tilde{z}\tilde{z}}$. Similarly, from (2.4*b*) we assume the dominant balance between $\tilde{p}_{\tilde{z}}/\rho$ and g. Here, unlike the usual boundary layer theory, we have taken into account the effect of gravity. This will couple the surface height h to the pressure, and will later turn out to be crucial for removing the singularities of the boundary layer approximation.

If we denote the characteristic radius and height by r_* and z_*, respectively, then the second dominant balance requires the characteristic pressure to be $\rho g z_*$. Then, the first balance relation requires $u_*/t_* = u_*^2/r_* = u_* w_*/z_* = \rho g z_*/(\rho r_*) = \nu u_*/z_*^2$ where u_* and w_* are typical radial and vertical velocities, respectively, and t_* is the characteristic time scale. The mass flux relation (2.6) requires that $u_* r_* z_* = q$ while the continuity equation (2.3) requires $u_*/r_* = w_*/z_*$. Solving these relations uniquely determines the characteristic scales:

$$\left.\begin{aligned} r_* &= (q^5 \nu^{-3} g^{-1})^{1/8} \simeq 2.7\,\mathrm{cm}, \qquad & z_* &= (q\nu g^{-1})^{1/4} \simeq 1.5\,\mathrm{mm}, \\ u_* &= (q\nu g^3)^{1/8} \simeq 12\,\mathrm{cm\,s^{-1}}, & w_* &= (q^{-1}\nu^3 g)^{1/4} \simeq 6.7\,\mathrm{mm\,s^{-1}}, \\ t_* &= (q\nu^{-1} g^{-1})^{1/2} \simeq 0.22\,\mathrm{s}, \end{aligned}\right\} \tag{2.7}$$

where the estimated values correspond to a typical set of parameters used in the experiments: $\nu \simeq 0.1\,\mathrm{cm^2\,s^{-1}}$ (for mixture of ethylene-glycol and water) and $Q \simeq 30\,\mathrm{cm^3\,s^{-1}}$, i.e. $q \simeq 5\,\mathrm{cm^3\,s^{-1}}$. The Reynolds number, defined as $R = u_* z_*/\nu = (q^3\nu^{-5} g)^{1/8}$, becomes $R \approx 18$. The Reynolds number at the nozzle outlet is much higher, but it becomes moderate near the jump. The values for r_* and z_* correspond well to a typical jump radius and fluid thickness in the experiments. Also, the predicted scaling can be experimentally tested by, for instance, measuring the dependence of the jump radius by changing the parameters such as q. In Bohr *et al.* (1993) evidence of the scaling and validity of the underlying assumption was given.

Using the characteristic scales (2.7), together with the pressure scale $p_* = \rho u_*^2$, we non-dimensionalize the full equations (2.4), then drop the terms involving the thin

https://doi.org/10.1017/S0022112003003744 Published online by Cambridge University Press

flow parameter: $\epsilon = z_*/r_* = (q^{-3}\nu^5 g^{-1})^{1/8} \simeq 0.05$, for the typical parameter values above. We also focus on stationary solutions in the rest of the section, and thus we obtain the simplified equations of motion:

$$uu_r + wu_z = -p_r + u_{zz}, \quad 0 = -p_z - 1. \tag{2.8a, b}$$

Correspondingly, within the error of $O(\epsilon^2)$, the dynamic boundary conditions (2.5) are just

$$p|_{z=h} = Wh_{rr}, \quad u_z|_{z=h} = 0. \tag{2.9a, b}$$

Here we have introduced the Weber number

$$W = \sigma z_*/(\rho u_*^2 r_*^2) = \sigma/(\rho g r_*^2) = \ell^2/(2r_*^2) = \sigma\rho^{-1}(q^{-5}\nu^3 g^{-3})^{1/4},$$

where $\ell = \{2\sigma/(g\rho)\}^{1/2}$ is the capillary length. For the parameter values above together with $\sigma \sim 70\,\mathrm{dyn\,cm^{-1}}$ (maximum), we estimate that $W \sim 0.01$ and $\ell \sim 3.8\,\mathrm{mm}$. Since W is small, we neglect it in the study of stationary states. On the other hand, it influences the dispersion of short waves, so should be included in the stability analysis of stationary states, possibly together with the neglected terms of $O(\epsilon^2)$ and higher in (2.8). Equations (2.8*b*) and (2.9*a*) with W set to zero yield the hydrostatic pressure:

$$p(r, z) = h(r) - z. \tag{2.10}$$

Combining (2.8*a*) and (2.10), we obtain the stationary boundary layer equation:

$$uu_r + wu_z = -h' + u_{zz}, \tag{2.11}$$

where the prime denotes the derivative with respect to r. This is supplemented by the dimensionless continuity equation and mass flux condition:

$$u_r + u/r + w_z = 0, \quad r\int_0^{h(r)} u(r, z)\,\mathrm{d}z = 1, \tag{2.12a, b}$$

respectively. The boundary conditions have been reduced to

$$u(r, 0) = w(r, 0) = 0, \quad u_z|_{z=h(r)} = 0. \tag{2.13a, b}$$

In addition to these conditions, boundary conditions in the radial direction also need to be specified. We do not elaborate on them, however, since the in- and outlet conditions arise naturally without the need for prescription when we obtain a simplified system.

The boundary layer equations (2.11)–(2.13) apparently form a closed system which could be solved by a marching numerical method from small to large r once inlet conditions have been specified. These equations could lead to separation, and indeed experiments show that there is a separation zone immediately behind a hydraulic jump. If a separation point, say at $r = r_s$, appears, the equations (2.11)–(2.13) will generically develop singularities of the Goldstein type, i.e. $u \sim (r_s - r)^{1/2}$ and $w \sim (r_s - r)^{-1/2}$, in the marching method. Higuera (1994, 1997) has shown, however, that the singularity can be removed by using both up- and downstream information for h' and solving iteratively.

In what follows we take a different approach based on integral methods (Grimson 1976). We do not aim to satisfy the boundary layer equations, but only their moments. Although heuristic, it leads to a simple set of ordinary differential equations (2.26), sufficient for avoiding a singularity at a separation point and approximating the overall flow.

https://doi.org/10.1017/S0022112003003744 Published online by Cambridge University Press

2.4. *Averaged equations*

Rather than solving the partial differential equation (2.11) itself, we shall be content with satisfying only the mass and momentum conservation laws, derived from averaging (2.11) over the transverse z-direction. To do this we make an ansatz for the radial velocity profile u. One might expect that the singularities at separation points do not contribute to the averages and do not cause any harm. Such an expectation is too naive as shown in the next section, since the model still shows singular behaviour near the jump if the simplest velocity profile is assumed. Nevertheless, we show in § 2.7 that the model becomes capable of going through the jump smoothly once enough flexibility is introduced in the assumed profile.

We first define the average velocity at r by $v = h^{-1}\int_0^h u(r,z)\,\mathrm{d}z$. The total mass flux condition (2.12b) can be written as

$$rhv = 1. \tag{2.14}$$

Next, for each fixed r, we integrate the radial momentum equation (2.11) over z from 0 to $h(r)$, and use the continuity equation (2.12a) with the surface boundary conditions (2.13). We obtain the averaged momentum equation

$$\frac{1}{rh}\left(r\int_0^h u^2\,\mathrm{d}z\right)' = -h' - \frac{1}{h}\,u_z|_{z=0}\,.$$

Using v and

$$G = \frac{1}{h}\int_0^h (u/v)^2\,\mathrm{d}z, \tag{2.15}$$

we obtain

$$v(Gv)' = -h' - \frac{1}{h}\,u_z|_{z=0}\,. \tag{2.16}$$

Equations (2.14) and (2.16) are the total mass and momentum equations.

2.5. *Similarity profile for u*

The simplest assumption for the radial velocity profile is a self-similar ansatz:

$$u(r,z)/v(r) = f(\eta), \tag{2.17}$$

where $\eta = z/h(r)$ takes values between 0 (bottom) and 1 (surface). Using (2.12a), the ansatz can be rewritten in the alternative form: $w(r,z) = \eta h' u(r,z)$. It is also equivalent to the requirement that the local inclination of the streamlines at (r,z) be proportional to $\eta h' = zh'(r)/h(r)$. Clearly, such an ansatz is too simple and 'rigid' to describe a flow with separation. However, this is the assumption used in the previous literature, and we summarize its consequences. For more details, see Bohr *et al.* (1993).

The conditions (2.13) and (2.14) now imply $f(0) = 0$, $f'(1) = 0$, $\int_0^1 f(\eta)\,\mathrm{d}\eta = 1$. They are not sufficient to uniquely determine f, and we choose one that is physically reasonable. Thus, a parabolic profile $f(\eta) = 3\eta - 3/2\eta^2$ is a simple candidate. Using this choice, $G = 6/5$ is a constant from (2.15), and (2.16) becomes

$$6vv'/5 = -h' - 3v/h^2. \tag{2.18}$$

Other choices for f lead to the same equation with different numerical coefficients. Since all such equations, corresponding to different choices of $f(\eta)$, can be further transformed to $vv' = -h' - v/h^2$ by suitably including numerical coefficients in the characteristic scales (2.7), the choice of f is not important in the study of qualitative behaviour and of parameter dependence.

https://doi.org/10.1017/S0022112003003744 Published online by Cambridge University Press

Using (2.14), the equation reduces to a single ordinary differential equation for $v(r)$:

$$v'\{v - 1/(v^2 r)\} = 1/(vr^2) - v^3 r^2. \tag{2.19}$$

This Kurihara–Tani equation was derived and studied in Tani (1949), in its dimensional form, and in Bohr *et al.* (1993). The results can be summarized as follows. To find a solution corresponding to a hydraulic jump, the velocity v should be large for small r, and decrease smoothly as r increases. However, the model does not have such a solution. The coefficient of v' on the left-hand side generically vanishes at some r where v' diverges. If (2.19) is solved in a parametric form on the (r, v)-plane, all solutions spiral around and into the fixed point $(r, v) = (1, 1)$, that is a stable focus in the plane. Therefore, one must still connect solutions in the interior and the exterior by means of, for example, a Rayleigh shock across which mass and momentum flux are conserved. When this is carried out, one finds that the shock occurs very close to $r = 1$ in the dimensionless coordinates, implying that the radius of the jump in the dimensional coordinates scales roughly as r_* in (2.7), i.e. $r_{\text{jump}} \propto q^{5/8}\nu^{-3/8}g^{-1/8}$. This scaling relation was compared to experiments (Bohr *et al.* 1993; Hansen *et al.* 1997) by changing q for several different ν. The radius of the jump did indeed scale with the mass flux q, but the exponent observed in the experiment was about 3/4 rather than 5/8. To explain the discrepancy, r_{jump} was calculated more accurately (Bohr *et al.* 1993). It was first proven that there is no solution for $v(r)$ to the Kurihara–Tani equation that extends to $r = \infty$. All solutions were found to diverge at some $r = r_{\text{end}}$ (constant) like $h \sim \{\log(r_{\text{end}}/r)\}^{1/4}$. By identifying this singularity as the end of the plate where the water runs off, one may always find the solution of (2.19) diverging at the end of the plate of a given radius $r = r_{\text{end}}$. By following the solution to smaller r, the solution before the jump and the position of the shock are uniquely determined assuming a connection via a Rayleigh shock. The shock location constructed in this way showed a good agreement (Bohr *et al.* 1993; Hansen *et al.* 1997) with the experiment.

2.6. *Profile with a shape parameter*

An ansatz more flexible than (2.17) must be used for resolving the flow pattern in the vicinity of the jump. We shall allow the function f in (2.17) to depend also on r. The simplest modification we can make is to assume $f = f(\eta, \lambda(r))$ so that the velocity profile is characterized by a single 'shape parameter' $\lambda(r)$. The approach follows the ideas developed by von Kármán and Pohlhausen (Schlichting 1979) for the usual boundary layer flow around a body. There, separation of the boundary layer can occur when the pressure gradient, imposed by the external inviscid flow, becomes adverse. In our case, there is no external flow, but there is a pressure gradient, along the bottom $z = 0$, that is proportional to $h'(r)$ due to the hydrostatic pressure (2.10). Thus, the possibility arises that the flow separates on $z = 0$ near the jump where h' is large and pressure is increasing in r, as in the usual boundary layer flow.

As an improvement over the parabolic profile, we approximate the velocity profile by the cubic:

$$u(r, z)/v(r) = a\eta + b\eta^2 + c\eta^3, \tag{2.20}$$

where a, b, c are now functions of r. Due to the boundary condition (2.13) and mass flux condition (2.14), the coefficients a, b and c can be expressed in terms of one parameter λ as, for example:

$$a = \lambda + 3, \quad b = -(5\lambda + 3)/2, \quad c = 4\lambda/3. \tag{2.21a–c}$$

https://doi.org/10.1017/S0022112003003744 Published online by Cambridge University Press

The separation condition $u_z|_{z=0} = 0$ is now equivalent to $a = 0$, or $\lambda = -3$. The u-profile is parabolic when $c = 0$, or $\lambda = 0$.

Now that we have two unknowns $h(r)$ and $\lambda(r)$, two equations are necessary. We use the averaged momentum equation (2.16) as the first equation. Note that G is now not a constant, but depends on the shape parameter λ. From (2.15), we obtain

$$G(\lambda) = 6/5 - \lambda/15 + \lambda^2/105. \tag{2.22}$$

Following the Kármán–Pohlhausen choice, we choose the second equation to be the momentum equation (2.11) evaluated at $z = 0$:

$$h' = u_{zz}|_{z=0}\,. \tag{2.23}$$

This connects the pressure gradient on $z = 0$ with λ. Using (2.21) and (2.22), the two equations (2.16) and (2.23) can be written as

$$v\{G(\lambda)v\}' = -h' - v(\lambda+3)/h^2, \quad h' = -v(5\lambda+3)/h^2, \tag{2.24a, b}$$

which can be simplified to

$$\{G(\lambda)v\}' = 4\lambda/h^2, \quad h' = -v(5\lambda+3)/h^2. \tag{2.25a, b}$$

Finally, eliminating v using (2.14), we obtain a non-autonomous system of two ordinary differential equations for $h(r)$ and $\lambda(r)$:

$$h' = -\frac{5\lambda+3}{rh^3}, \quad \frac{\mathrm{d}G}{\mathrm{d}\lambda}\lambda' = \frac{4r\lambda}{h} + G(\lambda)\frac{h^4-(5\lambda+3)}{rh^4}. \tag{2.26a, b}$$

This is the model for the stationary circular hydraulic jump. It does become singular, but only on the lines $h = 0$ and $\lambda = 7/2$, which does not cause any problems in describing a flow with a separated zone ($\lambda < -3$). We show in the next section that the highly simplified model does indeed contain solutions which describe the observed circular hydraulic jumps. Even though the model (2.25) was derived ignoring short wavelengths and surface tension, we will demonstrate below that (2.25) provides a very convincing description of the regions before the jump, after the jump and the jump itself. A similar approach using momentum and energy conservation was used in Arakeri & Rao (1996), but they did not succeed in finding continuous solutions through the jump.

2.7. *Numerical solution of the integrated model*

The model (2.26) can be solved as a boundary value problem by specifying two boundary conditions for different values of r. Thus we impose $(r_1, h_1(r_1))$ and $(r_2, h_2(r_2))$, $r_1 < r_2$, where the values are taken from the measured surface height data. There is no fitting parameter once they are chosen, and the function $h(r)$ and the shape parameter $\lambda(r)$ are determined. In particular, we do *not* need to specify the shape parameter as a part of the boundary conditions. This is an advantage of the simplified model since one no longer needs to specify the velocity profile at the inlet and/or outlet boundaries, which is not easy to do. In fact, we see that specifying both h and λ at one r, either inside the jump or outside, and solving (2.26) as an initial value problem is unstable. The system is extremely sensitive to the initial condition if one integrates (2.26) in the direction of increasing r from a small r or in the direction of decreasing r from a large r. Therefore, we choose r_1 and r_2 near 1, typically r_1 around 0.4–0.8 and r_2 around 1.2–1.6. Then, a straightforward shooting method from either boundary is sufficient to obtain a solution. After this is achieved, the solution

https://doi.org/10.1017/S0022112003003744 Published online by Cambridge University Press

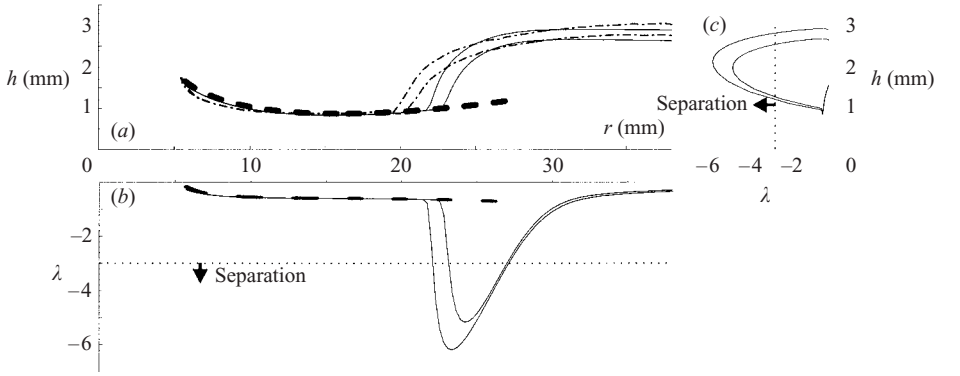


FIGURE 4. (*a*) Two surface height profiles of type I flow, taken from the experiment in figure 2 are shown as the dot-dashed curves. Numerical solutions of the model (2.25) are shown as solid curves, and show reasonable agreement. To obtain each of the numerical solutions, h values were read from the experimental data at $r = 11.8$ mm and $r = 30.0$ mm, then a boundary value problem was solved by the shooting method. The thick dashed curve represents an analytical approximation of the solutions before the jump, described in § 2.8.1. The formulae (2.30) and (2.31) show good agreement with one fitting parameter. (*b*) The computed shape parameter $\lambda(r)$, characterizing the velocity profiles, corresponding to the two numerical solutions in (*a*). The flow is separated behind the jump where $\lambda < -3$, and approaches the parabolic profile $\lambda = 0$ as r increases. Again, the dashed curve is an analytical approximation. (*c*) Two trajectories of (2.25) are shown in the (h, λ)-plane. They correspond to solid curves in (*a*) and (*b*).

is extended to $r < r_1$ and to $r > r_2$ by integrating (2.26) backwards from r_1 and forwards from r_2, respectively. Integrations in these directions are stable.

Figure 4(*a*) shows two solutions of such a boundary value problem. They correspond to the two type I solutions in figure 2, reproduced here as dot-dashed curves. From each curve the boundary data are taken at $\tilde{r}_1 = 11.8$ mm (corresponding to dimensionless value $r_1 = 0.42$) and $\tilde{r}_2 = 30.0$ mm ($r_2 = 1.07$). The computed solutions $h(r)$ corresponding to the data are shown as solid curves. Each curve shows a gradual decrease for small $\tilde{r}$ as $\tilde{r}$ increases, reaches a minimum at some $\tilde{r} \approx 15$ mm, and then undergoes a sharp jump at $\tilde{r} \approx 22$–23 mm, and a slow decay after the jump. The location of the jump is about 10% different in each case, and the slope behind the jump is noticeably different. However, the qualitative behaviour is captured well by the simple model. Figure 4(*b*) shows the shape parameter λ. The velocity profile changes suddenly almost simultaneously with the rapid increase of the surface height, and a region where $\lambda < -3$, corresponding to separation, is observed in each case. (If the downstream height is further reduced, however, the shape parameter λ does not reach $\lambda = -3$, and there is no separated region. Thus, our model predicts that a (weaker) jump without an eddy is possible. The flow near the bottom still decelerates just after the jump.) The parameter $\lambda(r)$ recovers and appears to converge to $\lambda = 0$ (the parabolic profile) as r becomes large. We emphasize again that the equations remain perfectly regular around the separation points.

The flow structure is more directly shown in figure 5, where the u-velocity profiles are computed from λ at equidistant locations in r. Since magnitudes of the velocity vary considerably between small and large r, the profiles are scaled by the average velocity, so that the profiles of $u(r, z)/v(r)$ are shown. The stream function ψ is computed from the definition $u = \psi_z/r$, $w = -\psi_r/r$. The dimensionless stream function varies from $\psi = 0$ on $z = 0$ to $\psi = 1$ on $z = h$. Inside the separated region

https://doi.org/10.1017/S0022112003003744 Published online by Cambridge University Press

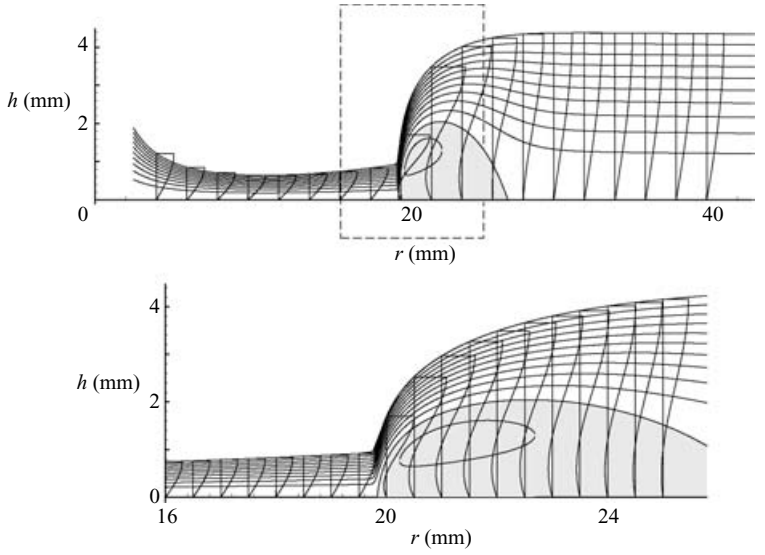


FIGURE 5. Visualization of the type I flow pattern based on the computed shape parameter $\lambda(r)$ from the model. The velocity profiles at equidistant locations in r are the horizontal component u, thus they are not tangential to the streamlines. Since magnitudes of the velocity vary greatly between small and large r, the profiles of $u(r, z)/v(r)$ are shown. The streamlines separate zones which carry 10% of the flow rate. A separation bubble is present in the range of r where $\lambda < -3$. Note the difference in the scales for the axes. The parameters differ from those of figure 4. They are: $Q = 33$ ml s^{-1} and $\nu = 1.4 \times 10^{-5}$ m^2 s^{-1}, corresponding to $r_* = 2.5$ cm, $z_* = 1.7$ mm, and $u_* = 16$ cm s^{-1}.

$\psi < 0$. The contours at $\psi = -0.1, 0, 0.1 \ldots, 1$ are shown in the figure: that is, a region between two neighbouring contour curves carries 10% of the mass flux.

The surface velocity U predicted from the model is shown in figure 6. The parameters are as in figure 5. The model again misses the location of the jump by about 20%, so measurements and the curve from the model are offset, but qualitative features are well reproduced. The velocity outside the jump is small and decays like $U \propto 1/r$, as can be seen from the log–log plot in the inset. This is consistent with an almost constant h and a nearly parabolic velocity profile, which we analytically demonstrate in the next section. On the other hand, the surface velocity decreases almost linearly before the jump. This region is harder to explain intuitively, but an analytical approximation is also obtained in the next section. At the jump a rapid, cusp-like drop in the velocity is noticed.

Finally, we discuss the dependence of the solutions on the external height h_{ext}. Both in experiments and in the model the height inside the jump is little affected by the change in the external boundary condition $h_2(r_2)$. The numerical solutions as well as the measured surface profiles in figure 4(a, b) apparently overlap in the interior to the jump. Of course, the two solutions must correspond to different trajectories of the model (2.25) and cannot collapse exactly onto a single curve. However, the closeness of the solution curves in the interior of the jump is the cause of the difficulty of solving the initial value problem starting from a small r.

If the external height is further increased, a transition from type I to II is observed in the experiment, as illustrated in figure 2 and figure 3. Unfortunately, no such transition is reproduced in the model when h_2 is increased. Instead, one finds a computed solution of the model similar to the ones in figure 4 even for a much

https://doi.org/10.1017/S0022112003003744 Published online by Cambridge University Press

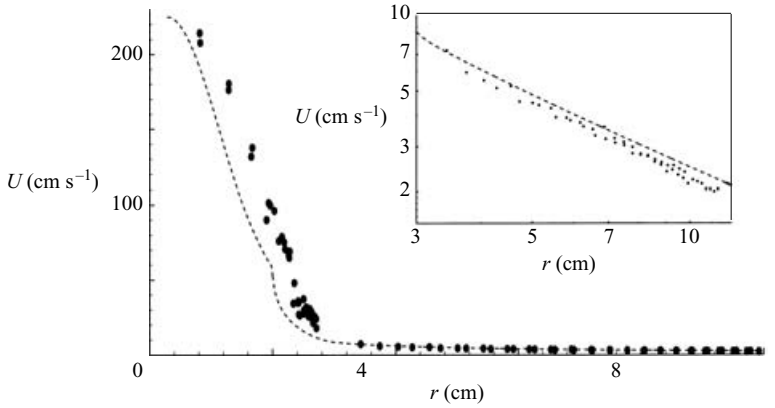


FIGURE 6. Comparison of the prediction from the model with surface velocity measurements by C. Ellegaard, A. E. Hansen, and A. Haaning (Bohr *et al.* 1996). The parameters are the same as in figure 5. Marker particles and a high-speed camera were used in order to obtain the surface velocity U shown as dots. The theoretical dotted curve was computed by finding a stationary solution $h(r)$ and $\lambda(r)$ of a boundary value problem using two data points taken from the measured surface profile (not shown). Although the location of the jump is about 20% in error, the model reproduces qualitative feature of the measurement very well. At small r, the velocity drops rapidly and almost linearly. It then shows a cusp-like drop at the jump, and decays gradually for large r. The final decay is proportional to $1/r$ as can be seen from the slope of about -1 in the log–log plot of the exterior region (inset).

larger h_2. A physical mechanism to 'break' the wave into a type II flow appears to be missing. In fact, a solution with a roller is prohibited by the model (2.25). The surface velocity on a roller is negative (inward). According to (2.21), the velocity at the surface is $U = v(a + b + c) = v(9 - \lambda)/3$, where $v > 0$ is the average velocity. Thus, $U < 0$ if and only if $\lambda > 9$. However, since we start with $\lambda \simeq 0$ and the line $\lambda = 7/2$ makes (2.25) singular, a solution with a roller is not possible. It seems likely that this behaviour can be traced back to the assumed pressure distribution (2.10) which does not provide any pressure gradient along the surface $z = h$. In a recent simulation of the circular hydraulic jump by Yokoi & Xiao (2000) pressure buildup just behind the jump is observed and claimed to be crucial in breaking the jump. The non-hydrostatic pressure arises partly due to the surface tension in (2.9*a*), but also due to the truncated viscous terms in (2.8) and (2.9). We do not know at present how best to extend our model to include the type II flows.

2.8. *Asymptotic analysis of the averaged model and Rayleigh's conservation laws*

In this section we approximate the solutions of (2.25) analytically. Two 'outer' regions are first considered: the region before the jump where r and h are small, and the one after the jump, where r is large and v is small. Moreover, we derive a single ordinary differential equation for the 'inner' region near the jump. Ideally, the three regions should be treated together using a matched asymptotic analysis in a limit of a flow parameter — the Reynolds number, for instance. However, such parameters are scaled out completely in (2.25). We use instead geometric parameters as expansion parameters, and treat the three regions separately. Our aim is to obtain a heuristic but explicit and useful expression in each region. For the two outer regions we show that the model (2.25) results in height profiles consistent with Watson (1964) and the Kurihara–Tani model. In addition, analysis in the inner region connects a previous model using a Rayleigh shock with our model through a parameter β which measures

https://doi.org/10.1017/S0022112003003744 Published online by Cambridge University Press

the degree of interaction between the pressure and the velocity fields. Everywhere in this section, quantities expected to be of order unity will be denoted by capital script letters.

2.8.1. *Outer solution* 1 (*before the jump*)

First, we analyse the region before the jump where the thickness of the fluid as well as the radius are small, compared to the exterior region. We denote the typical radius as θ, and treat it as a formal small parameter. We rescale the variables into $\mathscr{H}$, $\mathscr{R}$, and $\mathscr{V}$ as follows:

$$h = \theta^{\alpha}\mathscr{H}, \quad r = \theta\mathscr{R}, \quad v = \theta^{-1-\alpha}\mathscr{V}, \tag{2.27a–c}$$

and require consistent balance of the terms in (2.26) or, equivalently, (2.25). The rescaling for v in (2.27c) is chosen to ensure mass conservation (2.14) for all θ. In terms of the new variables, (2.25) can be written as

$$\theta^{-2-\alpha}\frac{\mathrm{d}}{\mathrm{d}\mathscr{R}}(G(\lambda)\mathscr{V}) = \theta^{-2\alpha}\frac{4\lambda}{\mathscr{H}^2}, \quad \theta^{\alpha-1}\frac{\mathrm{d}\mathscr{H}}{\mathrm{d}\mathscr{R}} = -\theta^{-3\alpha-1}\mathscr{V}\frac{5\lambda+3}{\mathscr{H}^2}. \tag{2.28a, b}$$

From the first equation the only consistent choice is to take $\alpha = 2$. Then, in order to balance the powers of θ on both sides of the second equation, we need

$$\lambda = -3/5 + \theta^8\Lambda_1 + \ldots. \tag{2.29}$$

The form is also motivated by figure 4 in which λ stays close to the value $-3/5$ before the jump. To find $\mathscr{H}(\mathscr{R})$ and the correction λ_1, substitute (2.29) into (2.28a). To the lowest order in θ we obtain $G(-3/5)(\mathscr{R}\,\mathrm{d}\mathscr{H}/\mathrm{d}\mathscr{R} + \mathscr{H}) = 12\mathscr{R}^2/5$, where $G(-3/5) = 1088/875 \simeq 1.243$. Solving this equation yields

$$\mathscr{H} = C_1/\mathscr{R} + 4\mathscr{R}^2/\{5G(-3/5)\}, \tag{2.30}$$

where C_1 is an arbitrary integration constant. The functional form, containing terms of $O(\mathscr{R}^{-1})$ and $O(\mathscr{R}^2)$, agrees with Watson's self-similar solutions (Watson 1964). We also compare the lowest-order term of θ in (2.28b), and find that $\Lambda_1 = (\mathscr{R}\mathscr{H}^3/5)(\mathrm{d}\mathscr{H}/\mathrm{d}\mathscr{R})$. By substituting $\mathscr{H}$ in (2.30) we obtain an approximate expression for λ:

$$\lambda = -3/5 + \theta^8\{\mathscr{H}^4/5 - 12\mathscr{R}^2\mathscr{H}^3/(25G(-3/5))\} = -3/5 + h^4/5 - 105r^2h^3/272. \tag{2.31}$$

We test the approximations (2.30) and (2.31) in figure 4. The dashed curves are the theoretical curves of $h(r)$ and $\lambda(r)$, shown in the dimensional coordinates. They match the numerical solutions and the measurements well before the jump. The one free parameter C_1 was fitted to be 0.25.

2.8.2. *Outer solution* 2 (*after the jump*)

Let us now consider the behaviour of (2.25) for large r. We introduce a formal large parameter Θ, and now rescale $r = \Theta\mathscr{R}$. If we moreover assume that the height is of order 1, i.e. $h = \mathscr{H}$, then the rescaling of the velocity is necessarily $v = \Theta^{-1}\mathscr{V}$ due to (2.12b). Using these new variables, (2.25) becomes

$$\Theta^{-2}\frac{\mathrm{d}}{\mathrm{d}\mathscr{R}}(G(\lambda)\mathscr{V}) = 4\lambda/\mathscr{H}^2, \quad \frac{\mathrm{d}\mathscr{H}}{\mathrm{d}\mathscr{R}} = -\mathscr{V}(5\lambda+3)/\mathscr{H}^2. \tag{2.32a, b}$$

In order to balance the terms in the first equation we choose

$$\lambda = \Theta^{-2}\Lambda_1 + \ldots. \tag{2.33}$$

This is again consistent with figure 4(b) where λ apparently tends to 0, corresponding to the parabolic profile. Then, the terms of order unity in the second equation are

https://doi.org/10.1017/S0022112003003744 Published online by Cambridge University Press

$\mathrm{d}\mathscr{H}/\mathrm{d}\mathscr{R} = -3/(\mathscr{R}\mathscr{H}^3)$ which has the solution

$$\mathscr{H} = \{12\log(\mathscr{R}_{\mathrm{end}}/\mathscr{R})\}^{1/4}, \tag{2.34}$$

where $\mathscr{R}_{\mathrm{end}}$ is an integration constant representing the radius where the height goes to 0. Thus, (2.25), as well as the simpler Kurihara–Tani model (2.18), becomes singular when $r \to \infty$. This seems to be a general property of models based on the boundary layer equations (Bohr *et al.* 1993). The absence of regular solutions for the system (2.11)–(2.13) when $r \to \infty$ was proved in Putkaradze & Rugh (1993). We have attributed this lack of asymptotic solutions to the influence of the finite size of the plate. Indeed, a solution with vanishing height such as (2.34) reminds one very much of a flow running off the edge of a circular plate.

The height $\mathscr{H}(\mathscr{R})$, given by equation (2.34), is a very slowly varying function of $\mathscr{R}$. There is a long regime $1 \ll \mathscr{R} \ll \mathscr{R}_{\mathrm{end}}$ where the height appears almost constant. In this intermediate regime the leading order of (2.32*a*) becomes $G(0)\mathrm{d}\{(\mathscr{R}\mathscr{H})^{-1}\}/\mathrm{d}\mathscr{R} = 4\Lambda_1/\mathscr{H}^2$ where $G(0) = 6/5$. Therefore,

$$\lambda = \Theta^{-2}\Lambda_1 = -\Theta^{-2}\frac{G(0)\mathscr{H}^2}{4}\left(\frac{1}{\mathscr{R}\mathscr{H}^2}\frac{\mathrm{d}\mathscr{H}}{\mathrm{d}\mathscr{R}} + \frac{1}{\mathscr{R}^2\mathscr{H}}\right) \approx \frac{3}{10r^2}\left(\frac{3}{h^3} - h\right). \tag{2.35}$$

We conclude that $\lambda(r) \propto 1/r^2 \to 0$ which explains the observed approach to the parabolic velocity profile for large r.

2.8.3. *Inner solution near the jump: conservation of momentum*

Finally, we analyse the region around the hydraulic jump. Recall that in the Kurihara–Tani theory (2.18) the jump was obtained by fitting a Rayleigh shock. In this section, we show that our model (2.26) is a natural generalization of that approach.

To do this we return to (2.24), and introduce a formal parameter β on the left-hand side of the second equation:

$$v\{G(\lambda)v\}' = -h' - v(\lambda+3)/h^2, \quad \beta h' = -(5\lambda+3)/(rh^3), \tag{2.36a, b}$$

where $v = 1/(rh)$. The second equation originated from (2.23), and inserting β on the left-hand side controls the degree of the interaction between the hydrostatic pressure and the velocity profile. (It turns out that β is also the length scale of the jump region.) Of course, the value $\beta = 1$ is the physical case, and the equations reduce to our model (2.24). However, since that case is analytically intractable, we consider the limiting case $\beta \to 0$ when there is only slight interaction between the pressure and the velocity fields.

In fact, setting $\beta = 0$ gives $\lambda = -3/5$ identically. Then (2.36*a*) becomes the Kurihara–Tani equation (2.18), except that the coefficient $6/5 = 1.2$ is changed to $G(-3/5) \approx 1.243$ here, since the profile is not parabolic. (As discussed before, the velocity profile is not so important in their model as long as it is self-similar.) Since the limit $\beta = 0$ is a singular limit, however, we carry out a more careful analysis as $\beta \to 0$.

In the Kurihara–Tani model a shock is needed to extend the solution from small to large values of r. Suppose the shock is situated at $r = r_0$. Consider a small region of size β around $r = r_0$, and rescale the coordinate as $r = r_0 + \beta\mathscr{X}$. Then, in the inner coordinate $\mathscr{X}$, (2.36) becomes

$$\frac{1}{r_0 h}\frac{\mathrm{d}}{\mathrm{d}\mathscr{X}}\left\{\frac{G(\lambda)}{r_0 h}\right\} = -\frac{\mathrm{d}h}{\mathrm{d}\mathscr{X}} + O(\beta), \quad \frac{\mathrm{d}h}{\mathrm{d}\mathscr{X}} = -\frac{5\lambda+3}{r_0 h^3} + O(\beta). \tag{2.37a, b}$$

https://doi.org/10.1017/S0022112003003744 Published online by Cambridge University Press

We see that $\lambda = -3/5$ with h an arbitrary constant are the only possible fixed points of (2.37). Thus the solutions must satisfy $\lambda \to -3/5$ for $\mathscr{X} \to \pm\infty$. This correctly matches the external solution before the jump, but not after the jump, where $\lambda \to 0$. (Note that the singularity of the outer solution after the jump (2.34), (2.35) for $r \to 0$ does not allow correct matching for $\mathscr{X} \to +\infty$ when $\beta \to 0$. Nevertheless, our method reproduces the structure of the separation zone quite well.) Equation (2.37a) can be integrated once, giving the momentum conservation: $G(\lambda)/(r_0^2 h) + h^2/2 = C_3$, with an integration constant C_3. Now we solve (2.37b) for λ, and substitute it into this equation. Using (2.22) in the form $G(\lambda) = \frac{1}{105}\left(\lambda - \frac{7}{2}\right)^2 + \frac{13}{12}$, we obtain an ordinary differential equation for h only:

$$\frac{1}{105}\left(\frac{r_0 h^3}{5}\frac{\mathrm{d}h}{\mathrm{d}\mathscr{X}} + \frac{41}{10}\right)^2 + \frac{13}{12} + \frac{r_0^2 h^3}{2} = C_3 r_0^2 h. \tag{2.38}$$

We look for a solution $h(\mathscr{X})$ with $h \to h_1$ as $\mathscr{X} \to -\infty$ and $h \to h_2$ as $\mathscr{X} \to +\infty$, where h_1 and h_2 are constants. Then, (2.38) with the first boundary condition determines the constant C_3 in terms of r_0 and h_1. Eliminating C_3, we obtain

$$\frac{1}{105}\left[\left(\frac{r_0 h^3}{5}\frac{\mathrm{d}h}{\mathrm{d}\mathscr{X}} + \frac{41}{10}\right)^2 h_1 - \left(\frac{41}{10}\right)^2 h\right] + \frac{13}{12}(h_1 - h) - \frac{r_0^2}{2} h_1 h (h_1^2 - h^2) = 0. \tag{2.39}$$

Inserting the second boundary condition into this equation yields a relation between h_1 and h_2, given r_0:

$$h_1 h_2^2 + h_1^2 h_2 - 2h_c^3 = 0, \tag{2.40}$$

where $h_c = (G(-3/5)/r_0^2)^{1/3}$ is the critical height for the circular hydraulic jump. In dimensional variables $\tilde{h}_c = (G(-3/5)q^2/g\tilde{r}_0^2)^{1/3}$, and is identical to the critical height that appeared in the Rayleigh shock, apart from the numerical factor and the influence of $\tilde{r}_0$ reflecting the radial geometry. The viscosity ν only enters in the coefficient of $\mathrm{d}h/\mathrm{d}\mathscr{X}$ in the dimensional version of (2.39), thus does not affect $\tilde{h}_c$.

Solving (2.40), we obtain an equation analogous to the shock condition (2.1):

$$h_2/h_1 = (-1 + \sqrt{1 + 8(h_c/h_1)^3})/2 = 2/(-1 + \sqrt{1 + 8(h_c/h_2)^3}). \tag{2.41}$$

It is easy to see that h_c is always between h_1 and h_2, i.e. $h_1 < h_c < h_2$ or $h_2 < h_c < h_1$. The Froude number in this case could naturally be defined as $F(\mathscr{X})^2 = (h_c/h(\mathscr{X}))^3$, but it is not clear whether F defined in this way can be a measure of super- and subcriticality since the governing equations are not the shallow water equations and therefore propagation of disturbances does not obey the well-known velocity $\sqrt{gh}$. It is still interesting to recover expressions like in the Rayleigh shock systematically in our laminar and viscous situation.

When h_1 is close to h_c, the final height h_2 is close to h_c as well. Then, the Froude number is close to unity for all $\mathscr{X}$, and the jump is weak, i.e. $h_c - h_1 = \delta \ll 1$. Then, we see from the balance of the terms in (2.39) that $h = h_c + \delta Y(\delta\mathscr{X})$. The leading balance reduces to $Y' = \gamma(1 - Y^2)$, with $\gamma = \frac{196875}{1312}(\frac{7}{17})^{2/3} r_0^{5/3} \approx 83.1 r_0^{5/3}$. Thus, in the weak jump limit, the height is given by $h(\mathscr{X}) = h_c + \delta \tanh(\delta\gamma\mathscr{X})$.

It is interesting to note that we can connect from h_1 at $\mathscr{X} = -\infty$ to h_2 at $\mathscr{X} = +\infty$ if $h_1 < h_2$, but not if $h_1 > h_2$, just like in the Rayleigh shock. This requirement comes from equation (2.39) self-consistently rather than making a hypothesis for the energy loss as in (2.2). To see this, consider the stability of the fixed points h_1

https://doi.org/10.1017/S0022112003003744 Published online by Cambridge University Press

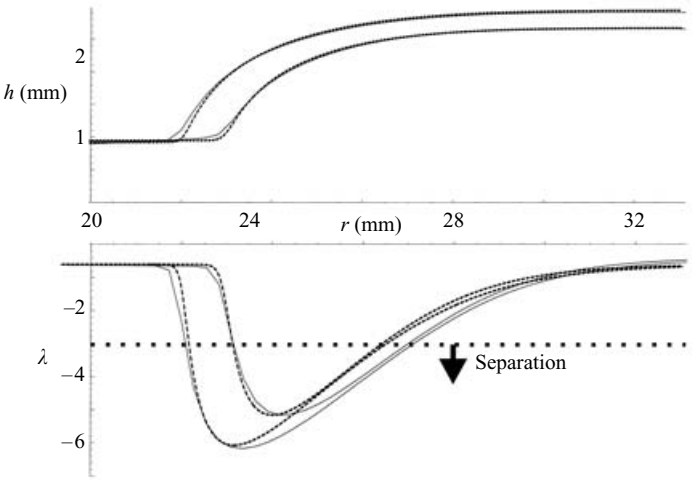


FIGURE 7. Comparison between the full numerical solution of (2.25), the same two solutions as in figure 4 shown as solid curves, and solutions of the asymptotic equation (2.39), shown as dashed curves. Even though the asymptotic analysis assumes $\beta \to 0$, the solutions compare fairly well with the full numerics corresponding to $\beta = 1$. The asymptotic analysis connects the model (2.25) with the Rayleigh shock condition. See text.

and h_2 with respect to the governing equation (2.39) for h. (Of course, this stability analysis is to study existence of stationary solutions, and not to study the stability of such solutions in the time-dependent theory.) Linearizing (2.39) around the uniform solutions h_i (where $i = 1, 2$), we obtain an equation for the perturbation δh_i in the height: $\mathrm{d}(\delta h_i)/\mathrm{d}\mathscr{X} = K_i \delta h_i$ where $K_i = 2625 r_0 \{2h_c^3 + h_1(h_1^2 - 3h_i^2)\}/(82 h_i^3 h_1)$. If $h_1 < h_c < h_2$, then $K_1 > 0 > K_2$, showing that the fixed point $h = h_1$ is unstable and $h = h_2$ stable. A trajectory departing from h_1 at $\mathscr{X} = -\infty$ and arriving at h_2 at $\mathscr{X} = +\infty$ is not prohibited, and we can indeed find such a trajectory, shown in figure 7. In contrast, if $h_1 > h_c > h_2$, then the stability of the fixed points is reversed, and there is no trajectory going from h_1 to h_2.

When $h_1 < h_c < h_2$ so that such a trajectory exists, the departure from h_1 is generally rapid, giving an impression of a 'sharp corner' at the beginning of the jump, and the arrival at h_2 is much smoother, as shown in figure 7. This is because the magnitude of the stability coefficient K_1 is large compared to that of K_2. The feature is most pronounced when h_1 is small (so h_2 is large). It vanishes as $(h_2 - h_1) \to 0$ when K_1 and K_2 both tend to zero.

In figure 7 we compare solutions of (2.39) with the two solutions of the full numerical solution of (2.25) shown in figure 4. The jump region is enlarged. Solutions of (2.39), shown as solid curves, are computed by fitting the values for h_1 and h_2, and solving the equation using r_0 obtained from (2.40). We chose an initial condition to be somewhere inside the jump, and integrated (2.39) forwards and backwards from it. Since (2.39) has a translational invariance with respect to $\mathscr{X}$, the initial condition fixes the location of the jump without affecting the shapes of h or λ. The analysis assuming $\beta \to 0$ performs surprisingly well against the numerical solution for $\beta = 1$. The size of the jump region is now of order β, i.e. unity, and the internal structure is non-trivial. The single ordinary equation (2.39) is capable of describing the eddy formation in this region.

https://doi.org/10.1017/S0022112003003744 Published online by Cambridge University Press

3. Flow down an inclined plane

3.1. *Introduction*

In this section we show the applicability of the method developed in § 2 in the two-dimensional Cartesian geometry. We consider a fluid stream running down an inclined plane under the action of gravity, following the same strategy to derive averaged partial differential equations in § 3.2. Models based on self-similar and one-parameter velocity profiles are compared.

Assuming stationarity, the equations reduce to systems of ordinary differential equations. An analogue of the circular hydraulic jump is sought in § 3.3. There is a unique equilibrium flow, corresponding to a fixed point in the stationary equations. It is, thus, impossible to find a solution with a jump which connect two equilibrium flows, as in Rayleigh's shock. We show that, in our viscous model, a solution with a jump which connects a *transient* flow to an equilibrium flow is possible if a shape parameter is included. It is quite difficult to study the stability of the solution, so we only study the dispersion relation around the equilibrium flow in § 3.4. The analysis still provides information on the limitations of the one-parameter model and on the criterion for super- or subcriticality of the flow.

Of course, the flow down an inclined plane has been a subject of great theoretical and practical importance, and has attracted the attention of many researchers. Starting with the pioneering work of Kapitsa & Kapitsa (1949), some of the major contributions to this field are found in Benjamin (1957), Benney (1966), Nakaya (1975), Pumir, Manneville & Pomeau (1983), Chang, Demekhin & Kopelevich (1993), Chang (1994), Liu & Gollub (1994), Lee & Mei (1996). These studies mostly deal with the time evolution of surface waves. Our one-parameter model is unsuited to time-dependent calculations of chaotic wave trains for instance, but is capable of finding solitary travelling fronts that could occur when the influx of fluid upstream is suddenly changed. It turns out, however, that these fronts are not analogous to the circular hydraulic jump in the sense that the velocity profiles deviates little from parabolic. In addition, the definition of super- or subcriticality is with respect to the front, and its criterion becomes trivial. Therefore, we describe these issues in the Appendix.

3.2. *Governing equations in the two reduced models*

Since the derivation of the two reduced models is analogous to the radial case, we simply write down the resulting equations in this geometry.

Take the x-axis in the downstream direction parallel to the plane inclined at an angle α (between 0 and $\pi/2$), and the y-axis in the perpendicular direction from the plate. The liquid surface is given by $y = h(x, t)$, and $v(x, t)$ is the average velocity across the layer from $y = 0$ to h. The continuity equation averaged over the thickness does not depend on the choice of the velocity profile, and becomes

$$h_t + (hv)_x = 0, \tag{3.1}$$

where $q = hv$ is the local flux. On the other hand, the averaged momentum equation depends on this choice. If we assume the self-similar profile analogously to the radial case, we obtain

$$(hv)_t + G(hv^2)_x = 3h/R - 3hh_x/(R\tan\alpha) - 3v/(Rh) + Whh_{xxx}, \tag{3.2}$$

where G is a constant for a chosen profile, and R and W are Reynolds and Weber numbers, respectively, suitable for this geometry. In particular, $R = v_*h_*/\nu = q_*/\nu = gh_*{}^3\sin\alpha/(3\nu^2)$ and $W = \sigma/(\rho h_* v_*{}^2) = 9\sigma/(\rho g h_*{}^2\sin^2\alpha)$, where the chosen

https://doi.org/10.1017/S0022112003003744 Published online by Cambridge University Press

characteristic values v_*, h_*, q_* are the average velocity, the depth, and the flux of the Nusselt flow. The value $G = 6/5$, corresponding to assuming the parabolic profile, is used for concreteness. This similarity model was originally considered by Shkadov and is often called the 'Shkadov model' (Prokopiou *et al.* 1991; Chang *et al.* 1993; Chang 1994).

If we assume a variable one-parameter profile for u instead, with a third-order polynomial as before, then we obtain

$$(hv)_t + (hv^2G(\lambda))_x = 4v\lambda/(Rh), \quad h_x \cot\alpha = 1 - v(5\lambda + 3)/(3h^2) + WRh_{xxx}/3. \tag{3.3a, b}$$

For (3.3*b*) the momentum equation evaluated on the bottom is again chosen. These equations were reported earlier (Bohr *et al.* 1997). Also, Ruschak & Weinstein (2001) recently tested a one-parameter family of conditions as candidates for (3.3*b*). They found evaluation on the bottom yielded the best quantitative agreement with their extensive computations of the full Navier–Stokes and boundary layer equations.

In the following we call (3.2) with (3.1) the 'similarity model' and (3.3) with (3.1) the 'one-parameter model'. Both models inherit the trivial uniform solution (Nusselt solution) from the complete Navier–Stokes model: $h = v = q \equiv 1$, and, for the one-parameter model, $\lambda \equiv 0$ (the parabolic profile).

3.3. *Stationary jumps*

In the Appendix we seek solutions for the two models that propagate down the plane with a constant velocity $c \geqslant 0$. Travelling waves ($c > 0$) studied in previous work can be adequately described by the models. In addition, the one-parameter model possesses a different family of stationary solutions which we describe in this section. Thus, we focus on the special case $c = 0$ by dropping the time derivatives in the models. The continuity equation (3.1) becomes just $q = hv = 1$, which is used to eliminate v from the other equations. The two models are now reduced to ordinary differential equations that can be treated as dynamical systems where x is the independent variable. The presence of surface tension makes the order of the equations higher and makes it difficult to find interesting trajectories. We set $W = 0$, hoping that singular effects when W is small but finite are contained only in short-scale structures such as small oscillations on the surface. Any trajectories of the reduced dynamical systems correspond to stationary flows, but the most interesting ones are those convergent to the fixed point (the Nusselt flow) when $x \to \infty$, i.e. sufficiently far downstream.

The similarity model now reduces to a single equation:

$$\mathrm{d}h/\mathrm{d}x = (h - 1)(h^2 + h + 1)/(h^3/\tan\alpha - 2R/5). \tag{3.4}$$

Due to the first-order nature of the equation, trajectories convergent to the equilibrium point as $x \to \infty$ do so only monotonically. Such trajectories can be shown to exist only when $R\tan\alpha > 5/2$. Figure 8(*a*) shows three trajectories for $\alpha = 3^\circ$ and three values of R in this regime ($R > 47.7$). For smaller R, the fixed point is repelling, thus we conclude that the model is too simple to describe any jump structure.

On the other hand, the one-parameter model results in

$$(h^{-1}G(\lambda))_x = 4\lambda/(Rh^2), \quad h_x \cot\alpha = 1 - (5\lambda + 3)/(3h^3). \tag{3.5a, b}$$

This is a two-dimensional system, and the fixed point $h = 1$, $\lambda = 0$ is always a saddle. We can easily compute the trajectory convergent to the fixed point as its stable manifold. The one approaching from smaller h is chosen and plotted in

https://doi.org/10.1017/S0022112003003744 Published online by Cambridge University Press

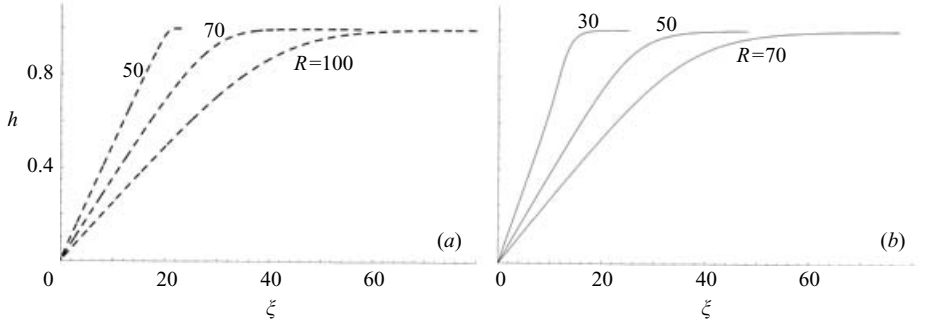


FIGURE 8. Computed stationary solutions for $\alpha = 3^\circ$ and $c = 0$. Dashed curves are solutions of the similarity model (3.4) for $R = 50$, 70, and 100. Solid curves are solutions of the one-parameter model (3.5) for $R = 30$, 50, and 70. A larger R corresponds to a slower convergence to the equilibrium flow $h = 1$. These solutions do not show any shock-like structure.

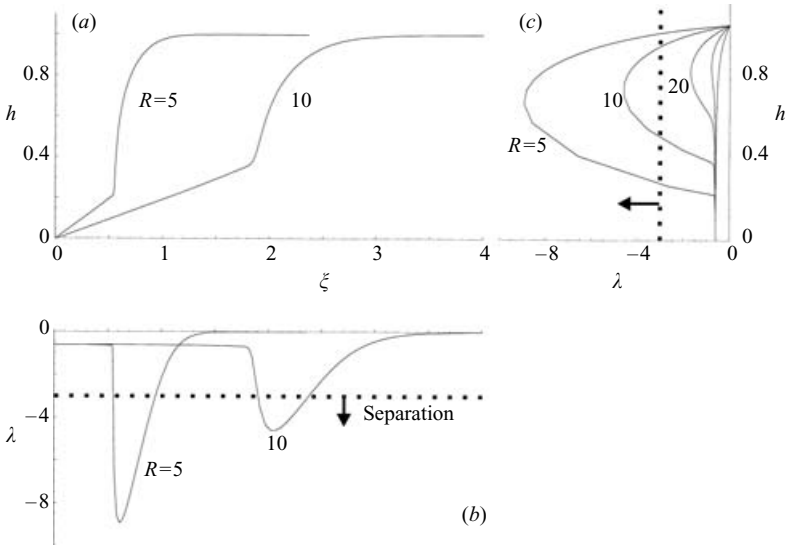


FIGURE 9. (*a*) Computed height h of the stationary solutions for the one-parameter model (3.5) using $\alpha = 3^\circ$, $c = 0$, and $R = 5$ and 10. A shock-like structure is visible, with a fast shooting flow in front of it and a slow equilibrium flow behind. (*b*) The shape parameter λ corresponding to the solutions in (*a*) shows separation, $\lambda < -3$, in both solutions. (*c*) Corresponding trajectories on the phase portrait of h versus λ. In addition to the two solutions for $R = 5$ and 10, three more solutions for $R = 20$, 30, and 50 are shown. An excursion to small λ before convergence to the fixed point at (0, 1) is visible for trajectories with small R.

figure 8(*b*). The trajectories are monotonically approaching the equilibrium height if R is sufficiently large. They are qualitatively identical to the ones from the similarity model. However, for smaller R, we obtain a different type of trajectory as shown in figure 9. Both the height profile and the shape parameter vary rapidly at a certain x, creating a jump structure. This is the two-dimensional version of the jump we obtained for the circular hydraulic jump. The phase portrait in (*c*) demonstrates how unstable the upstream part of the flow is. Trajectories make large excursions for small R. This type of solution does not connect two equilibrium flows, but an upstream

https://doi.org/10.1017/S0022112003003744 Published online by Cambridge University Press

transient flow to a downstream equilibrium one. It could be realized, for instance, as a stationary flow exiting a sluice gate placed at some $x > x_0$. (A full-scale channel flow such as a river certainly requires turbulence modelling, but a miniature laminar experiment can be performed (Ruschak & Weinstein 2001).)

We can analyse the solutions asymptotically near x_0 by assuming that $h \sim A(x-x_0)$ as $x \to x_0+0$. Then, we obtain from mass conservation $v \sim 1/\{A(x-x_0)\}$. Substituting these into (3.5*b*) yields $\lambda \sim -\frac{3}{5}\{1 - A^3(1 - A\cot\alpha)(x - x_0)^3\}$. Finally, comparing coefficients of the dominant terms in (3.5*a*) determines $A = 12/\{5RG(-3/5)\} \approx 1.93/R$ where $G(\lambda)$ is given by (2.22).

When R is large and A is small, λ increases at the point $x = x_0$. Then, the solution reaches the parabolic profile $\lambda = 0$ monotonically. On the other hand, when R is small, A is large and λ may decrease at x_0. Then, the trajectory makes an excursion to smaller λ, sometimes into the separation zone $\lambda < -3$, before recovering toward $\lambda = 0$. Therefore, the condition to obtain the second type is $A\cot\alpha > 1$, or $R\tan\alpha < 12/\{5G(-3/5)\} \simeq 1.93$. Figures 8(*b*) and 9 confirm this criterion.

3.4. *Dispersion around the equilibrium flow*

We now come back to the time-dependent equations, and discuss the linear stability of the Nusselt flow in the two models. By linearizing the similarity model (3.1), (3.2) around $h = v = 1$ and decomposing infinitesimal disturbances into Fourier modes as $\delta h, \delta v \sim \exp\{\mathrm{i}(kx - \omega t)\}$, we obtain the dispersion relation

$$\omega_\pm = -\frac{3\mathrm{i}}{2R} + \frac{6}{5}k \pm \sqrt{D_0}, \tag{3.6}$$

where the discriminant is given by

$$D_0 = -\frac{9}{4R^2} + \frac{27\mathrm{i}}{5R}k + 3k^2\left(\frac{2}{25} + \frac{1}{R\tan\alpha}\right) + Wk^4.$$

Treating the one-parameter model (3.1), (3.3) similarly, the dispersion relation is found to be

$$\omega_\pm = -\frac{6\mathrm{i}}{5R} + \frac{61}{50}k \pm \frac{3}{5}\sqrt{D_1}, \tag{3.7}$$

where

$$D_1 = -\frac{4}{R^2} + \frac{178\mathrm{i}}{15R}k + \left(\frac{421}{900} + \frac{20}{3R\tan\alpha}\right)k^2 + \frac{\mathrm{i}}{9\tan\alpha}k^3 + \frac{20W}{9}k^4 + \frac{\mathrm{i}RW}{27}k^5.$$

Note that this model also has only two dispersion branches because (3.3*b*) does not include time derivatives.

Unfortunately, the one-parameter model behaves spuriously in the short-wave limit. For large k, (3.7) becomes $\omega_\pm \sim \pm k^{5/2}\sqrt{\mathrm{i}W/75}$ if $W > 0$, or $\omega_\pm \sim \pm k^{3/2}\sqrt{\mathrm{i}/(25\tan\alpha)}$ if $W = 0$. In either case one of the branches is unstable, irrespective of R or α. We have been unable to find a natural way to prevent this unphysical behaviour. This restricts the validity of the one-parameter model only in the stationary situations. The difficulty may not be surprising since short waves are not well represented by the boundary layer approximation we started with. Nevertheless, the similarity model, originating from the same approximation, behaves reasonably in this limit (see the Appendix), and there is still room for a better model that can deal with time-dependent formation of a jump.

In the long-wave limit $k \to 0$ where the models *are* valid approximations, both dispersion relations are qualitatively identical. It is interesting to note that the waves

https://doi.org/10.1017/S0022112003003744 Published online by Cambridge University Press

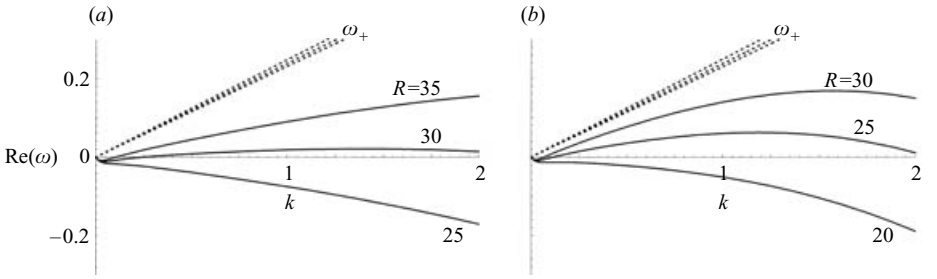


FIGURE 10. Real part of the dispersion relation showing the propagation of disturbances on the equilibrium flow. (*a*) Similarity model using (3.6) for $R = 25$, 30 and 35. (*b*) One-parameter model using (3.7) for $R = 20$, 25 and 30. In both models $\alpha = 5^\circ$ and $W = 0.01$ are fixed. Three dashed and solid curves correspond to the ω_+ and ω_- branches, respectively, of the dispersion relation. The ω_+ has a positive slope, or group velocity, for all k, while the ω_- branch has positive slope only when R is large. However, for large enough R, the region of k in which both branches have positive slopes extends from small k corresponding to wavelengths beyond the system size to large k with wavelengths smaller than the thickness of the flow. In this case the flow is essentially supercritical since disturbances are all carried away downstream.

corresponding to ω_- always propagate upstream, indicating that *the flow is subcritical irrespective of* R. This is quite unexpected since disturbances should not propagate upstream for sufficiently large R. An explanation can be found in figure 10 where the real parts of ω_+ (dashed curves) and ω_- (solid) are plotted against k for three different R. Note the rapid bending of the ω_- branches near $k = 0$ when R becomes sufficiently large. The deviation from the long-wave limit approximation becomes significant even for small k. For small R the slope is everywhere negative, thus the flow is subcritical. On the other hand, for sufficiently large R, the curves have a positive slope for a wide range of k. Since the system length limits the smallest k in practice, the flow becomes essentially supercritical. This defines a natural distinction between the super- and subcritical flows within a *viscous* model.

4. Conclusions

In this article we have presented a simple but fairly quantitative method of reducing flows with strongly deformed free surfaces to a manageable system of equations. By assuming a 'flexible' velocity profile whose shape parameter is another dependent variable, flows with an internal eddy can be described. In the radial geometry our results compare well with experiments and we have obtained analytic expressions for different parts of the circular hydraulic jump.

The same method is also used to construct a minimal model to describe a jump structure in the flow down an inclined plane. Introducing a shape parameter is found to be crucial. Only for small enough Reynolds numbers are sharp deformations in the surface and the internal velocity profile possible.

The dispersion relation around the equilibrium flow for the reduced models is then studied. We have shown that for sufficiently long waves supercritical flow is not possible, but waves with intermediate lengths can make the flow essentially supercritical.

Both the value and the limitations of our method lie in its simple and heuristic nature. It seems to be hard to systematically push the method to higher order. We have considered assuming fourth-order polynomials for u with two shape parameters, but the resulting equations are hard to study, and it is not apparent that improvements

https://doi.org/10.1017/S0022112003003744 Published online by Cambridge University Press

can be gained. A few promising methods have been developed for thin film flows recently. Roberts (1996) used the centre manifold theory and obtained a two-variable model which captures qualitatively new effects absent in the similarity model with the parabolic profile. This appears to be a sound way to derive reduced equations systematically although it is not clear if it can be expanded to a model with three variables, required for describing eddies. Ruyer-Quil & Manneville (1998) took a different integral approach using weighted residuals of the lateral momentum equation. This is similar to the method presented here, but higher-order equations for the flow down an inclined plane show good linear stability characteristics around the equilibrium flow. However, the equations become quite complicated and it is not easy to find solutions with a jump in their equations.

To describe the jump region more accurately a systematic expansion such as application of the triple-deck theory (Sobey 2000) is certainly more appropriate. Our failure to predict the type I to II transition in the circular jump and to suppress instability of the short waves also indicate the limitations of our method and a need for a more elaborate treatment of the terms neglected in the boundary layer approximation. However, such a detailed analysis would be complicated, and it would be difficult, if not impossible, to couple it to the flow outside the jump region and to derive an approximation of the surface profile as we did, heuristically, here. The simplicity of our method would also enable one to model even more complicated flows including separation bubbles.

The core part of this work was carried out at the Centre for Chaos & Turbulence Studies (CATS) at the Niels Bohr Institute, to which authors are grateful for an inspiring environment. S. W. thanks the Institute for Mathematics & its Applications (IMA) of the University of Minnesota, and V. P. acknowledges the University of Chicago for their hospitality. Research supported in part under Grant-in-Aid for Scientific Research of JSPS; NSF grants. DMR 9415604 and DMR 9808595, and MRSEC; and the Sandia National Laboratory's SURP grant.

Appendix. Application of the integral method for the flow down an inclined plane

This Appendix supplements § 3, and compares the similarity and the one-parameter models for describing the flow down an inclined plane. It demonstrates that the one-parameter model is consistent in describing the travelling wave solutions studied previously. In particular, kink-like solitary wave solutions (Pumir *et al.* 1983) going from one constant height h_1 to another h_2 are found in the model.

In addition, we compute the dispersion relations of the equilibrium flow for different wavelengths, and discuss super- and subcriticality of the flow.

A.1. *Stationary solutions in a moving coordinate frame*

Both stationary solutions studied in § 3.3 and travelling waves can be sought as stationary solutions in a moving coordinate system with a suitable constant velocity c. Thus, we use the travelling wave coordinate $\xi = x - ct$, and rewrite the models within this frame. The mass conservation (3.1) used in both models becomes $-ch_\xi + (hv)_\xi = 0$ which can be integrated to

$$-ch + hv \equiv Q = \text{constant}, \tag{A 1}$$

where Q is the mass flux, viewed in the moving frame. (Note that the flux $q(x, t)$ in the laboratory frame is, in general, not a constant. The discharge at the inlet must

https://doi.org/10.1017/S0022112003003744 Published online by Cambridge University Press

be varied in time accordingly.) The flow must approach the uniform equilibrium flow $h = 1$ in the $\xi \to \infty$ limit. Suppose it also approaches another equilibrium flow $h = h_2$ in the $\xi \to -\infty$ limit. Then, using the mass conservation $q = hv = h^3$, the condition becomes $-ch_2 + h_2^3 = Q = -c + 1$.

Of course, $h_2 = 1$ is a solution of this equation. In this case we might still be able to find a non-trivial solution of a pulse-like solitary wave form. Such solutions have previously been studied well (Chang *et al.* 1993; Chang 1994), and we do not further consider this type of solution. For a solution other than $h_2 = 1$, we need

$$c = h_2^2 + h_2 + 1. \tag{A 2}$$

The positive solution is $h_2 = (-1 + \sqrt{4c - 3})/2$ for $c > 1$.

When $c > 1$ two different equilibrium solutions exist, and we hope to find a kink-like solution which connects the two limiting flows. However $c > 1$ is only the *necessary* condition for its existence. Sufficiency for the existence depends on the models and the parameters: R, α, and c. In § A.2 we shall clarify the parameter regime for finding such solutions. It turns out that the velocity profiles in this type of solution do not deviate much from parabolic even in the one-parameter model. In this sense they correspond to somewhat 'mild' jumps in terms of the flow structure.

In § A.3 we find another family of solutions which approaches $h = 1$ as $\xi \to \infty$ when $c < 1$. These solutions do not start from an equilibrium state at $\xi = -\infty$. Instead, they are only valid for ξ larger than some value ξ_0. In the similarity model they are not interesting since they approach $h = 1$ smoothly. However, within the one-parameter model, an abrupt change is developed in both the surface and velocity profiles, sometimes with separation. We interpret this solution, when $c = 0$, as the analogue of the circular hydraulic jump in the Cartesian geometry.

We set $W = 0$ here for the same reason as discussed in § 3.3. Under this assumption we convert the averaged models into the moving coordinate frame at velocity c. Equation (3.2) in the similarity model becomes:

$$-c(hv)_\xi + \tfrac{6}{5}(hv^2)_\xi + 3hh_\xi/(R\tan\alpha) = -3v/(Rh) + 3h/R.$$

Using the condition (A 1), v can be eliminated. We obtain a first-order differential equation for h:

$$\frac{\mathrm{d}h}{\mathrm{d}\xi} = \frac{15}{R}\frac{(h-1)(h^2+h+1-c)}{c^2h^2 - 6(1-c)^2 + 15h^3/(R\tan\alpha)}. \tag{A 3}$$

Similarly, (3.3) in the one-parameter model is converted to

$$-c(hv)_\xi + (hv^2G(\lambda))_\xi = 4v\lambda/(Rh), \quad h_\xi\cot\alpha = 1 - v(5\lambda+3)/(3h^2) \tag{A 4a, b}$$

to be solved with (A 1). One variable, for instance v, can be eliminated so that the system becomes two-dimensional for h and λ.

In the following sections we treat these averaged models as 'dynamical systems', and view ξ as a time-like variable. Fixed points of these systems correspond to the uniform, equilibrium solutions of the original time-dependent equations. Note that stability in terms of the variable ξ is not equivalent to temporal stability of the original time-dependent equations.

A.2. *Travelling wave solutions*

Due to the relationship (A 2), which is a one-to-one map between c and h_2 in the range $c > 1$, we may treat h_2 or c as the primary parameter interchangeably. Using h_2 as a parameter corresponds physically to varying the height and discharge upstream

https://doi.org/10.1017/S0022112003003744 Published online by Cambridge University Press

and then observing the corresponding change in the wave velocity. The condition $c > 1$ is equivalent to $h_2 > 0$, and $h_2 > 1$ if $c > 3$. The two regimes $h_2 > 1$ and $h_2 < 1$ are qualitatively different. For $h_2 > 1$ the discharge at $\xi \to -\infty$ is increased, and a forward-facing front travels downstream. As we shall see in this section, this state exists for small enough R. In contrast, $h_2 < 1$ corresponds to a backward-facing front which is found to exist for large enough R but seems to us very likely unstable. Thus, we concentrate on the case $h_2 > 1$ in the following. Note that if we used the geometric mean of the up- and downstream heights $(\tilde{h}_1\tilde{h}_2)^{1/2}$ as the characteristic length, we would obtain equations whose symmetric appearance makes it easy to study the forward- and backward-facing fronts simultaneously. However, we have chosen to scale by the downstream height $\tilde{h}_1$ in order to treat the travelling waves as well as the stationary jumps.

A.2.1. *The similarity model*

Since (A 3) is a first-order autonomous ordinary differential equation, the necessary condition for the existence of a heteroclinic orbit starting from $h_2(>1)$ and arriving at $h = 1$ is that the fixed point $h = 1$ is stable and h_2 is unstable. By linearization, the fixed point $h = 1$ is found to be stable if

$$c^2 - 6(1-c)^2 + 15/(R\tan\alpha) > 0, \tag{A 5}$$

or

$$R\tan\alpha < 15/\{6(1-c)^2 - c^2\} = 15/(5h_2^4 + 10h_2^3 + 3h_2^2 - 2h_2 - 1) \equiv f_1(h_2), \tag{A 6}$$

where the denominator is positive for $c > 3$. Similarly, h_2 is found to be unstable if

$$R\tan\alpha < 15h_2/\left(-h_2^4 - 2h_2^3 + 3h_2^2 + 10h_2 + 5\right) \equiv f_2(h_2). \tag{A 7}$$

The denominator of f_2 vanishes only at $h_2 = h_2^{\max} \approx 2.13$ for the region $h_2 > 1$. If $h_2 > h_2^{\max}$, then $f_2 < 0$ and (A 7) cannot be satisfied. We discard this region of h_2. For $1 < h_2 < h_2^{\max}$ one finds that $f_2(h_2) > 1 > f_1(h_2)$. Thus, the necessary condition for the existence is simply (A 6). Once the necessary condition is fulfilled, sufficiency is guaranteed. To see this, we only need to ensure that the denominator on the right-hand side of (A 3) does not vanish in the region $1 < h < h_2$. Suppose it vanished at h_s, then we would have $c^2h_s^2 - 6(1-c)^2 + 15h_s^3/(R\tan\alpha) = 0$. Comparison with (A 5) gives $c^2(1-h_s^2) + 15(1-h_s^3)/(R\tan\alpha) > 0$. It is clear that $h_s > 1$ is impossible. Thus, $h_s < 1$, and there is no vanishing denominator in $1 < h < h_2$. In figure 11(a) we show computed solutions of (A 3) for three different Reynolds numbers. The parameters α and h_2 are fixed, such that (A 6) becomes $R < 6.95$. Within this range, a larger R makes the propagating front sharper.

A.2.2. *The one-parameter model*

We can eliminate v from (A 1) and (A 4), and think of trajectories on the phase portrait for (h, λ). We look for a heteroclinic orbit starting from a fixed point $(h_2, 0)$ and arriving at $(1, 0)$ as $\xi \to \infty$. It is necessary for its existence that the point $(h_2, 0)$ has at least one unstable direction and $(1, 0)$ has at least one stable direction. Linearizing around the equilibrium point as $h = h_e + \delta h$ and $\lambda = 0 + \delta\lambda$, where $h_e = 1$ or h_2, we obtain $(\delta h_\xi, \delta\lambda_\xi)^{\mathrm{T}} = \boldsymbol{J}(\delta h, \delta\lambda)^{\mathrm{T}}$ with the determinant of the 2×2 Jacobian matrix $\boldsymbol{J}$ calculated to be $\det \boldsymbol{J} = 60(c - 3h_e^2)\tan\alpha/(Rh_e^7)$. For the point $(h_2, 0)$ we have $c - 3h_e^2 = 1 + h_2 - 2h_2^2 < 0$ when $h_2 > 1$. This means that $\det \boldsymbol{J} < 0$ for $h_2 > 1$, and the fixed point is always a saddle, having exactly one unstable direction.

For the point $(1, 0)$ we have $\det \boldsymbol{J} > 0$ since $c - 3h_e^2 = h_2^2 + h_2 - 2 > 0$ when $h_2 > 1$. Thus, we also need the trace of the Jacobian for $h_e = 1$ which can be shown to be

https://doi.org/10.1017/S0022112003003744 Published online by Cambridge University Press

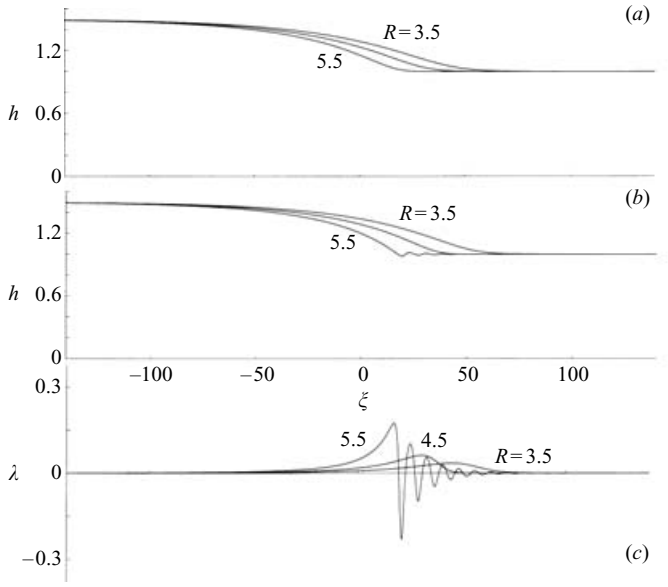


FIGURE 11. Computed examples of the travelling wave solutions connecting two equilibrium states. Here, the angle of the plane $\alpha = 2^\circ$, and the height $h \to h_2 = 1.5$ as $\xi \to -\infty$, corresponding to the front velocity $c = 4.75$. Three solutions for $R = 3.5$, 4.5 and 5.5 are shown. (*a*) Height h from solution of the similarity model (A 3). The front becomes steeper as R increases. (*b*) Height h from solution of the one-parameter model (A 4). The curves are quite similar to the ones in (*a*) except for the oscillation in the shallower side when R becomes close to a critical value. (See text.) (*c*) Shape parameter λ corresponding to the solutions in (*b*). They deviate from the parabolic profile $\lambda = 0$ and oscillate (for $R = 5.5$), but only slightly. This explains the similarity between (*a*) and (*b*).

$\mathrm{tr}\boldsymbol{J} = -60/R + (33 - 61c + 25c^2)\tan\alpha$. For the stability of $(1, 0)$ we need $\mathrm{tr}\boldsymbol{J} < 0$. Since $33 - 61c + 25c^2 > 0$ for $c > 3$, this condition becomes

$$R\tan\alpha < 60/(33-61c+25c^2) = 60/\left(-3-11h_2+14h_2^2+50h_2^3+25h_2^4\right) \equiv f_s(h_2). \quad \text{(A 8)}$$

When this is satisfied, the fixed point is locally attracting, and a trajectory may reach it from any direction. Indeed, we find numerically that the condition (A 8) also seems to be sufficient. For any R and α in the range (A 8), a heteroclinic solution was found. Computed solutions for three different values of R are shown in figure 11(b, c). The parameters α and h_2 are identical to the ones used for the similarity model in figure 11(a). The condition (A 8) yields $R < 5.59$. The height profiles in (*b*) are essentially identical to the ones in (*a*). This is because the shape parameter λ shown in (*c*) does not deviate much from $\lambda = 0$, the parabolic profile.

In figure 11(b, c), the solution is oscillatory around $h = h_1$ and $\lambda = 0$ for $R = 5.5$. This is a feature seen when R becomes close to the critical value given by (A 8). It happens when the type of the fixed point $(1, 0)$ changes from a stable node to a stable focus. The point is a focus when $\det\boldsymbol{J} > (\mathrm{tr}\boldsymbol{J})^2/4$, which is equivalent to $f_+(h_2) < R\tan\alpha < f_-(h_2)$, where $f_\pm(h_2) = 60/(-7 - 9h_2 + 16h_2^2 + 50h_2^3 + 25h_2^4 \pm 2\sqrt{5D})$, and $D = 2+3h_2-9h_2^2-19h_2^3+3h_2^4+15h_2^5+5h_2^6$. It can be seen that $f_+(h_2) < f_s(h_2) < f_-(h_2)$ for $h_2 > 1$. Therefore, a heteroclinic solution can be found and exhibits oscillations in a small region $f_+(h_2) < R\tan\alpha < f_s(h_2)$. In figure 11$(b, c)$ this condition corresponds to $4.81 < R < 5.59$, so only the solution for $R = 5.5$ shows oscillations.

https://doi.org/10.1017/S0022112003003744 Published online by Cambridge University Press

A.3. *Linear stability of equilibrium states*

It is quite difficult to carry out a linear stability analysis around the stationary solutions with a jump and travelling wave solutions found so far. They have non-uniform profiles obtained only numerically and some of the solutions have singular points beyond which they cannot be continued. Moreover, the inlet boundary condition can strongly affect the stability properties of the solutions. We shall therefore focus on the linear geometry, and only study the stability of the equilibrium flow $h \equiv$ constant. The results are, however, expected to be applicable to the equilibrium flow sufficiently far downstream of the jump in the stationary solutions and to flows sufficiently up- and downstream of the moving front in case of the travelling wave solutions. Since the dispersion relation scales with the chosen characteristic length, as described in § A.3.3, we only need to consider the flow $h \equiv 1$. Both the similarity model (3.2) and the one-parameter model (3.3) are considered, including the surface tension term which is expected to be relevant (Pumir *et al.* 1983) for stability. One of our aims is, of course, to judge when infinitesimal disturbances grow and when they decay, but their propagation velocities are also of particular interest. By comparing the velocities to a reference velocity, which is zero for the stationary jump and $c(>3)$ for the travelling wave, we are able to classify different parts of the solutions as either super- or subcritical.

The first step is to linearize the models around the fixed point $h = v = 1$ and, for the one-parameter model, $\lambda = 0$. Putting the infinitesimal disturbances of the form $\delta h, \delta v \sim \exp\{\mathrm{i}(kx - \omega t)\}$, into the equations, we obtain (3.6) for the similarity model, and (3.7) for the one-parameter model.

A.3.1. *Long-wave limit*

We first study the long-wave limit $k \to 0$ by taking only the lowest-order terms in k. For the similarity model, the dispersion relation (3.6) becomes

$$\omega_+ = 3k + \mathrm{i}k^2(R - \cot\alpha) + O(k^3), \quad \omega_- = -\frac{3\mathrm{i}}{R} - \frac{3}{5}k - \mathrm{i}k^2(R - \cot\alpha) + O(k^3). \tag{A 9a, b}$$

As $k \to 0$, the group velocities $\mathrm{d}\omega_+/\mathrm{d}k \to 3$ and $\mathrm{d}\omega_-/\mathrm{d}k \to (-3/5)$. Therefore, waves corresponding to ω_- propagate upstream, and *the flow is subcritical irrespective of* R. By studying the dominant imaginary components of $\omega_\pm$, we also find that the reverse propagating branch ω_- is always stable, i.e. the disturbances decay, for small enough k whereas the forward propagating branch ω_+ is stable only for small enough Reynolds number satisfying $R\tan\alpha < 1$.

The limiting dispersion is identical in the one-parameter model apart from numerical coefficients. For small k, (3.7) becomes $\omega_+ = 3k + \mathrm{i}k^2(5R/4 - \cot\alpha) + O(k^3)$, and $\omega_- = -12\mathrm{i}/(5R) - 14k/25 - \mathrm{i}k^2(5R/4 - \cot\alpha) + O(k^3)$. Thus, the flow is always subcritical since the long waves in the ω_- branch propagate upstream with velocity $-14/25$. Again, this branch is stable for any R while the ω_+ branch is stable only for small Reynolds numbers: $R\tan\alpha < 4/5$.

A.3.2. *Intermediate range of k*

It is quite unexpected that the flow is subcritical for any R. One would intuitively expect that disturbances cannot propagate upstream for sufficiently rapid flows. An explanation can be found by a more careful study of the dispersion relations (3.6) and (3.7), or, in particular, the discriminants D_0 and D_1.

https://doi.org/10.1017/S0022112003003744 Published online by Cambridge University Press

We first consider the similarity model. If the $O(k^2)$ term dominates in D_0, then the corresponding group velocities become $c_\pm = \mathrm{d}\omega_\pm/\mathrm{d}k \approx 6/5 \pm \sqrt{6/25 + 3/(R\tan\alpha)}$. Both c_+ and c_- become positive for

$$R\tan\alpha > 5/2. \tag{A 10}$$

We attempt to estimate such a range of k. For brevity we assume $R\tan\alpha \ll 25/2$ so that the coefficient of k^2 in D_0 can be approximated by $3/(R\tan\alpha)$. If the magnitude of the $O(k^2)$ dominates in D_0, then we must have $3k^2/(R\tan\alpha) \gg 9/(4R^2)$, $27k/(5R)$, Wk^4, that is,

$$\max\{\sqrt{3\tan\alpha/(4R)}, (9\tan\alpha)/5\} \ll k \ll \sqrt{3/(RW\tan\alpha)}. \tag{A 11}$$

Using $R = 30$, $\alpha = 5^\circ$ and $W = 0.01$, for instance, the condition (A 10) and (A 11) gives a window $0.16 \ll k \ll 10.7$ in which we can hope that the $O(k^2)$ term dominates.

Rather than attempting a more accurate estimate of the zone, we demonstrate that such an interval can be in fact quite long, by plotting the real part of $\omega_\pm(k)$ for (3.6) in figure 10(a). Three different values of R are used while α and W are fixed. The ω_+ branch, shown as dashed curves, has a positive slope for any k. Both phase and group velocities of this branch are positive. On the other hand, the ω_- branch, shown as solid curves, qualitatively changes with R. For $R = 25$ its slope appears to be negative for all k, indicating a subcritical flow. However, for a larger R there is an interval of k in which the slope becomes positive. In the limit $k \to 0$, the branch still has a negative slope in accordance with the analysis of the long-wave limit in the previous section. However, the subcritical region near $k = 0$ can be very small. One sees in figure 10(a) that the curve already has a positive slope when $k > 0.05$ and $R = 35$. The slope continues to be positive until $k = 2$, corresponding to a wavelength of half the thickness of the equilibrium flow. Since the system length is finite in practice, the subcritical flow in the $k \to 0$ limit cannot be achieved, and the flow becomes essentially supercritical for all the wavenumbers observed. This defines the super- and subcritical flows within our viscous model, and confirms the intuitive picture of having a supercritical flow when the flow is sufficiently rapid.

The situation is qualitatively identical in the one-parameter model. As the corresponding equations to (A 10) and (A 11), we obtain $R\tan\alpha > 20/11$, and

$$\max\left\{\sqrt{\frac{3\tan\alpha}{5R}}, \frac{50\tan\alpha}{89}\right\} \ll k \ll \min\left\{\frac{60\tan\alpha}{R}, \sqrt{\frac{3}{RW\tan\alpha}}, \frac{180}{R^2W\tan\alpha}\right\},$$

respectively. Again using $R = 30$, $\alpha = 5^\circ$ and $W = 0.01$, the interval becomes $0.05 \ll k \ll 0.18$. The upper limit comes from the $O(k^3)$ term in D_1, and is estimated to be rather small since we have only compared the magnitudes. In fact, when we plot the real part of the dispersion relation (3.7) in figure 10(b), we find that the ω_- branch has a positive group velocity for a much longer range of k. The supercritical flow near the $k = 0$ limit is very small once again if R becomes as large as $R = 25$.

A.3.3. *Super- and subcriticality for moving fronts*

The intermediate-k behaviour enables us to decide whether a given equilibrium flow is 'inherently' super- or subcritical. This distinction is made based on wave velocities with respect to the laboratory frame. A more classical distinction of the two types arises in the context of shock theory, as reviewed in § 2.1. In this case velocities are measured with respect to a moving front; we call the flow 'supercritical' if the group velocity of all the waves is less than the front velocity c, and 'subcritical' if there is

https://doi.org/10.1017/S0022112003003744 Published online by Cambridge University Press

a wave component with group velocity larger than c. Here, we briefly note that the averaged equations can describe this traditional classification, too.

Take a moving front such as the one shown in figure 11. We concentrate on the long-wave limit $k \to 0$. For $\xi \to \infty$ the flow approaches an equilibrium flow with $h = 1$. Linear waves propagate forwards and backwards with the group velocities $\mathrm{d}\omega_+/\mathrm{d}k = 3$ and $\mathrm{d}\omega_-/\mathrm{d}k = -3/5$ according to the dispersion relation for the similarity model (A 9). This is a subcritical situation in the laboratory frame, but, since the front velocity is $c = 1 + h_2 + h_2^2 > 3$, both these waves propagate into the front. Therefore, the flow is supercritical with respect to the front.

To derive the dispersion relation of the equilibrium flow with height h_2 for $\xi \to -\infty$, consider rescaling the height by h_2. That is, we use this height as the characteristic length so that a wavenumber k must be multiplied by h_2. Since the flow rate is $q_2 = h_2^3$, the velocity has to be scaled by $q_2/h_2 = h_2^2$. Thus, the group velocities for this flow in the laboratory frame are $\mathrm{d}\omega_+/\mathrm{d}k = 3h_2^2$ and $\mathrm{d}\omega_-/\mathrm{d}k = -3h_2^2/5$. It is easy to show that $3h_2^2 > c = 1 + h_2 + h_2^2$ for $h_2 > 1$. Thus, one wave component propagates into the front while the other moves away from it so that the flow behind the front is subcritical.

Therefore, the moving front has a supercritical flow on the shallower side and a subcritical flow on the deeper side, and can be regarded as a classical shock. Using the one-parameter model instead of the similarity model is qualitatively identical. The super- and subcriticality for travelling waves for the similarity model were previously pointed out by Prokopiou *et al.* (1991), Chang *et al.* (1993), Chang (1994).

A.3.4. *Short-wave limit*

We now come back to the stationary equilibrium flow, and study the dispersion relation in the short-wave range.

Since the derivation of the averaged equations relies on the assumption of predominantly horizontal flow, it is not our aim to accurately resolve wave components when k is large. We only hope that the short waves decay so that they do not interfere with meaningful dynamics when we simulate the time-dependent model. We have already stated in § 3.4 that the one-parameter model performs poorly in this respect.

However, this trouble cannot be solely attributed to weakness of the boundary layer approximation. In fact, the dispersion relation of the similarity model (3.6), derived under the same approximation, behaves reasonably even in the large-k limit, as follows. If $W > 0$, then it can be approximated as $\mathrm{Re}\,\omega_\pm = \pm\sqrt{W}k^2 + O(k)$, and $\mathrm{Im}\,\omega_\pm = -3/(2R) + O(k^{-1})$. Thus, short waves in (3.2) are damped out. If we set $W = 0$, the dispersion relation for large k is $\omega_\pm = c_\pm k - 3\mathrm{i}(c_\pm - 3)/\{2R(c_\pm - 6/5)\} + O(k^{-1})$ where $c_\pm$ is the velocity of the corresponding wave given by $c_\pm = 6/5 \pm \sqrt{6/25 + 3/(R\tan\alpha)}$. Since $c_- < 6/5$, the branch ω_- is always stable, as can be seen from this equation. On the other hand, since $c_+ > 6/5$, the condition for the stability of the branch ω_+ is $c_+ < 3$, which is equivalent to $R\tan\alpha < 1$. For a large R the equilibrium state is no longer stable, but this is reasonable in the absence of surface tension.

There is the possibility that this short-wave property may be combined with a shape parameter to make a model that can deal with time-dependent formation of jump structures.

REFERENCES

Arakeri, J. H. & Rao, A. 1996 On radial film flow on a horizontal surface and the circular hydraulic jump. *J. Indian Inst. Sci.* **76**, 73–91.

https://doi.org/10.1017/S0022112003003744 Published online by Cambridge University Press

Benjamin, T. B. 1957 Wave formation in laminar flow down an inclined plane. *J. Fluid Mech.* **2**, 554–574.

Benney, D. J. 1966 Long waves on liquid films. *J. Maths & Phys.* **45**, 150–155.

Blackford, B. L. 1996 The hydraulic jump in radially spreading flow: A new model and new experimental data. *Am. J. Phys.* **64**, 164–169.

Bohr, T., Dimon, P. & Putkaradze, V. 1993 Shallow-water approach to the circular hydraulic jump. *J. Fluid Mech.* **254**, 635–648.

Bohr, T., Ellegaard, C., Hansen, A. E. & Haaning, A. 1996 Hydraulic jumps, flow separation and wave breaking: an experimental study. *Physica* B **228**, 1–10.

Bohr, T., Ellegaard, C., Hansen, A. E., Hansen, K., Haaning, A., Putkaradze, V. & Watanabe, S. 1998 Separation and pattern formation in hydraulic jumps. *Physica* A **249**, 111–117.

Bohr, T., Putkaradze, V. & Watanabe, S. 1997 Averaging theory for the structure of hydraulic jumps and separation in laminar free-surface flows. *Phys. Rev. Lett.* **79**, 1038–1041.

Bowles, R. I. & Smith, F. T. 1992 The standing hydraulic jump: theory, computations, and comparisons with experiments. *J. Fluid Mech.* **242**, 145–168.

Brechet, Y. & Néda, Z. 1999 On the circular hydraulic jump. *Am. J. Phys.* **67**, 723–731.

Carter, J. E. & Wornom, S. F. 1975 Solutions for incompressible separated boundary layers including viscous-inviscid interaction. *NASA-SP* 347, pp. 125–150.

Chang, H.-C. 1994 Wave evolution on a falling film. *Annu. Rev. Fluid Mech.* **26**, 103–136.

Chang, H.-C., Demekhin, E. A. & Kopelevich, D. I. 1993 Nonlinear evolution of waves on a vertically falling film. *J. Fluid Mech.* **250**, 433–480.

Chow, V. T. 1959 *Open-Channel Hydraulics*. McGraw-Hill.

Craik, A. D. D., Latham, R. C., Fawkes, M. J. & Gribbon, P. W. F. 1981 The circular hydraulic jump. *J. Fluid Mech.* **112**, 347–362.

Ellegaard, C., Hansen, A. E., Hansen, K., Haaning, A., Marcussen, A., Bohr, T., Lundbek Hansen, J. & Watanabe, S. 1998 Creating corners in kitchen sinks. *Nature* **392**, 767.

Ellegaard, C., Hansen, A. E., Hansen, K., Haaning, A., Marcussen, A., Bohr, T., Lundbek Hansen, J. & Watanabe, S. 1999 Cover illustration: polygonal hydraulic jumps. *Nonlinearity* **12**, 1–7.

Gajjar, J. S. B. & Smith, F. T. 1983 On hypersonic self-induced separation, hydraulic jumps and boundary layers with algebraic growth. *Mathematika* **30**, 77–93.

Godwin, R. P. 1993 The hydraulic jump. *Am. J. Phys.* **61**, 829–832.

Goldstein, S. 1948 On laminar boundary-layer flow near a position of separation. *Quart. J. Mech. Appl. Maths* **1**, 43–69.

Grimson, J. 1976 *Advanced Fluid Dynamics and Heat Transfer*. McGraw Hill.

Hansen, S. H., Hørlück, S., Zauner, D., Dimon, P., Ellegaard, C. and Creagh, S. C. 1997 Geometric orbits of surface waves from a circular hydraulic jump. *Phys. Rev.* E **55**, 7048–7061.

Higuera, F. J. 1994 The hydraulic jump in a viscous laminar flow. *J. Fluid Mech.* **274**, 69–92.

Higuera, F. J. 1997 The circular hydraulic jump. *Phys. Fluids* **9**, 1476–1478.

Ishigai, S., Nakanishi, S., Mizuno, M. & Imamura, T. 1977 Heat transfer of the impinging round water jet in the interference zone of film flow along the wall. *Bull. JSME* **20**, 85–92.

Kapitsa, P. L. & Kapitsa, S. P. 1949 Wave flows of thin layers of a viscous fluid. In *Collected Works by P.L. Kapitsa*, pp. 690–709, Pergamon (1965).

Kurihara, M. 1946 On hydraulic jumps (Hanemizu ni tuite no ichi kosatsu). *Rep. Res. Inst. Fluid Engng* (*Kyusyu Imper. Univ. Ryutai Kogaku Kenkyusho Kiyou*) **3**, 11–33, in Japanese.

Landau, L. D. & Lifshitz, E. M. 1987 *Fluid Mechanics*. Pergamon.

Lee, J.-J. & Mei, C. C. 1996 Stationary waves on an inclined sheet of viscous fluid at high Reynolds and moderate Weber numbers. *J. Fluid Mech.* **307**, 191–229.

Liu, J. & Gollub, J. P. 1994 Solitary wave dynamics of film flows. *Phys. Fluids* **6**, 1702–1712.

Liu, X. & Lienhard V, J. H. 1993 The hydraulic jump in circular jet impingement and in other thin liquid films. *Exps. Fluids* **15**, 108–116.

Marcussen, A. 1999 Det hydrauliske spring. MSc thesis, Roskilde University, in Danish.

Nakaya, C. 1975 Long waves on a thin fluid layer flowing down an inclined plane. *Phys. Fluids* **18**, 1407–1412.

https://doi.org/10.1017/S0022112003003744 Published online by Cambridge University Press

Nakoryakov, V. E., Pokusaev, B. G. & Troyan, E. N. 1978 Impingement of an axisymmetric liquid jet on a barrier. *Intl J. Heat Mass Transfer* **21**, 1175–1184.

Olsson, R. G. & Turkdogan, E. T. 1966 Radial spread of a liquid stream on a horizontal plate. *Nature* **211**, 813–816.

Oron, A., Davis, S. H. & Bankoff, S. G. 1997 Long-scale evolution of thin liquid films. *Rev. Mod. Phys.* **69**, 931–980.

Prandtl, L. 1904 Über flüssigkeitsbewegungen bei sehr kleiner Reibung. In *Verhandl. III. Intl Math. Kongr. Heidelberg*, pp. 484–491, in German.

Prokopiou, Th., Cheng, M. & Chang, H.-C. 1991 Long waves on inclined planes at high Reynolds numbers. *J. Fluid Mech.* **222**, 665–691.

Pumir, A., Manneville, P. & Pomeau, Y. 1983 On solitary waves running down an inclined plane. *J. Fluid Mech.* **135**, 27–50.

Putkaradze, V. & Rugh, H. H. 1993 Non-analyticity of the boundary layer flows with a free surface. *Niels Bohr Inst. Rep.* NBI-92-09.

Rayleigh, Lord 1914 On the theory of long waves and bores. *Proc. R. Soc. Lond*, A **90**, 324–328.

Roberts, A. J. 1996 Low-dimensional models of thin film fluid dynamics. *Phys. Lett.* A **212**, 63–71.

Ruschak, K. J. & Weinstein, S. J. 2001 Developing film flow on an inclined plane with a critical point. *Trans. ASME*: *J. Fluids Engng* **123**, 698–702.

Ruyer-Quil, C. & Manneville, P. 1998 Modeling film flows down inclined planes. *Eur. Phys. J.* B **6**, 277–292.

Schlichting, H. 1979 *Boundary Layer Theory*. McGraw Hill.

Sobey, I. J. 2000 *Introduction to Interactive Boundary Layer Theory*. Oxford University Press.

Stoker, J. J. 1957 *Water Waves*. Interscience.

Tani, I. 1949 Water jump in the boundary layer. *J. Phys. Soc. Japan* **4**, 212–215.

Yokoi, K. & Xiao, F. 2000 Relationships between a roller and a dynamic pressure distribution in circular hydraulic jumps. *Phys. Rev.* E **61**, R1016–R1019.

Watson, E. J. 1964 The radial spread of a liquid jet over a horizontal plane. *J. Fluid Mech.* **20**, 481–499.

Whitham, G. B. 1974 *Linear and Nonlinear Waves*. Wiley.

https://doi.org/10.1017/S0022112003003744 Published online by Cambridge University Press